JOURNAL OF PETROLOGY | VOLUME 43 | NUMBER 10 | PAGES 1885–1908 | 2002

Dissolution of Corundum and Andalusite in H_2O-Saturated Haplogranitic Melts at 800°C and 200 MPa: Constraints on Diffusivities and the Generation of Peraluminous Melts

ANTONIO ACOSTA-VIGIL*, DAVID LONDON, THOMAS A. DEWERS AND GEORGE B. MORGAN VI

SCHOOL OF GEOLOGY AND GEOPHYSICS, UNIVERSITY OF OKLAHOMA, NORMAN, OK 73019, USA

RECEIVED FEBRUARY 28, 2001; REVISED TYPESCRIPT ACCEPTED MARCH 28, 2002

The mechanisms and kinetics of equilibration between peraluminous minerals and granitic melt were investigated experimentally by the dissolution of corundum and andalusite into H_2O-saturated metaluminous haplogranitic melt at 800°C and 200 MPa. Mineral and haplogranitic glass rods were juxtaposed inside platinum capsules, and then subjected to experimental conditions for times ranging from 12 to 2900 h. Upon melting, the mineral–melt interface retreats with the square root of time. The composition of the melt at the interface changes with time, but its ASI [aluminum saturation index = molar $Al_2O_3/(CaO + Na_2O + K_2O)$] remains constant at $\sim 1{\cdot}20$ after 480 h. This value is close to the ASI of an H_2O-saturated haplogranitic melt in equilibrium with corundum or andalusite, which may indicate that the composition of the melt at the interface follows the liquidus of these minerals in the system. Sodium and potassium diffuse rapidly uphill across the entire length of the charge towards the interface, resulting in a rapid and uniform increase in ASI throughout the entire melt column. This uphill diffusion of alkalis is due to coupling with excess aluminum entering the melt at the interface, and involves long-range communication in the melt via chemical potential gradients. The evolution of oxide concentration profiles with time suggests that sodium, potassium, and a combination of aluminum and alkalis constitute three directions in composition space along which diffusion is uncoupled directions (eigenvectors) in this system. The aluminum–alkali eigenvector has a molar Al/(Na + K) ratio of $\sim 1{\cdot}20$; its Na/K ratio, however, changes with the composition of the liquid and with time as the entire melt column approaches equilibrium. The solubility of H_2O shows a positive correlation with the excess aluminum content of melt, but conclusions about the stoichiometry of H_2O in the aluminum–alkali eigenvector could not be obtained from our results. We propose that some H_2O may provide charge balance for excess aluminum. Multicomponent diffusion models yield eigenvalues for the corresponding aluminum–alkali eigenvector of $0{\cdot}3 \times 10^{-10}$ to $1{\cdot}9 \times 10^{-10}$ cm^2/s. Calculated effective binary diffusion coefficients for Al_2O_3 are higher, $1{\cdot}0 \times 10^{-9}$ to $3{\cdot}6 \times 10^{-9}$ cm^2/s. These diffusion coefficients are used to calculate equilibration times between peraluminous minerals and granitic melts in a model system in which two grains of corundum or andalusite 1 cm apart are connected via a narrow melt column. At the conditions of the experiments, diffusive equilibrium through initially metaluminous H_2O-saturated melt would be attained within $\sim 10^1$–10^2 years. At H_2O activity well below saturation of the melt, lower diffusivity of all components may increase the time to equilibration to $\sim 10^4$–10^5 years, approaching possible time frames for the generation and extraction of crustal melts.

KEY WORDS: *dissolution experiments; corundum; andalusite; haplogranite; chemical diffusion; ASI; peraluminous*

INTRODUCTION

Diffusion is one of the main mass transport mechanisms in silicate liquids, and it is the means by which magmas ultimately achieve chemical and isotopic equilibrium. Because of this, diffusion studies are essential in two

*Corresponding author. Telephone: (405) 325-3253. Fax: (405) 325-3140. E-mail: acosta@hoth.gcn.ou.edu

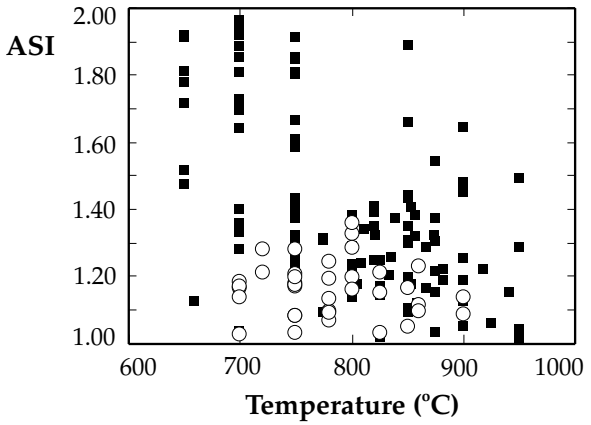

Fig. 1. ASI vs temperature for experimental glasses of granitic composition (■) and leucosomes and leucogranitic dikes in crustal anatectic terranes (○). The experimental glasses coexist with one or more strongly peraluminous minerals. The leucosomes and leucogranitic dikes are considered as melts derived from the surrounding peraluminous migmatites.

ways. First, as noted by Bowen (1921, 1928), the rate of diffusion is an important control on whether or not equilibrium is reached during igneous processes (e.g. partial melting, interaction between magmas and xenoliths, mixing between magmas, and crystallization from a melt). Information about diffusivity can, therefore, place constraints on the time frame of these geological processes. Second, diffusion studies can provide basic understanding of melt production at an atomic scale by revealing likely melt species. The knowledge of speciation, in turn, provides information on melt structure that is needed to form a rigorous basis from which thermodynamic and transport models for the melt can be constructed.

The partial melting of peraluminous protoliths should produce peraluminous melts in which the ASI [aluminum saturation index = molar $Al_2O_3/(CaO + Na_2O + K_2O)$] should have values >1 and should increase with rise in temperature as refractory peraluminous phases increasingly dominate the melting assemblage. Surprisingly, natural rock compositions and experimental results appear to contradict this expectation. Partial melts derived from the anatexis of strongly peraluminous protoliths can be metaluminous to weakly peraluminous, as for example at Ronda in the Betic Cordilleras of southeastern Spain, where tourmaline- and cordierite-bearing leucogranite dikes with a mean ASI value of $\sim$1·05 appear to be derived from strongly peraluminous migmatites (e.g. Torres-Roldán, 1983; Tubía, 1988; Acosta-Vigil *et al.*, 2001). Published data (Fig. 1) suggest a broad negative correlation between ASI and temperature for experimental granitic melts and natural granitic leucosomes, which coexist with one or more strongly peraluminous phases (Weber *et al.*, 1985; Wickham, 1987; Le Breton & Thompson, 1988; Vielzeuf & Holloway, 1988; Barbey *et al.*, 1990; Patiño Douce & Johnston, 1991; Holtz *et al.*, 1992*a*; Watt & Harley, 1993; Bea *et al.*, 1994; Obata *et al.*, 1994; Barbero *et al.*, 1995; Gardien *et al.*, 1995; Icenhower & London, 1995, 1996; Braun *et al.*, 1996; Patiño Douce & Beard, 1996; Montel & Vielzeuf, 1997; Acosta, 1998; Patiño Douce & Harris, 1998). To explain the unexpected low ASI values of partial melts derived from very aluminous protoliths, we consider two hypotheses: (1) that the kinetics of dissolution of strongly peraluminous minerals is slow on the time scales of melt generation and extraction; (2) that the solubility of excess alumina in melt is a function of melt composition, i.e. the solubility of excess alumina is coupled in some way with the other components of the melt (e.g. Clemens & Wall, 1981; Patiño Douce, 1992; London *et al.*, 2001). In this paper we experimentally investigate the mechanisms and kinetics of dissolution of corundum and andalusite into H_2O-saturated metaluminous haplogranitic melt [the 200 MPa H_2O-saturated minimum composition of Tuttle & Bowen (1958)] at 800°C, which is representative of crustal anatectic temperatures. We choose corundum because it is the alumina-saturating phase in (slightly) quartz-undersaturated melts (i.e. at temperatures above the liquidus surface of quartz), and andalusite because it is prevalent in siliceous S-type granitic rocks (e.g. Clarke *et al.*, 1976; Kontak *et al.*, 1984; Noble *et al.*, 1984; Morgan *et al.*, 1998). By ascertaining how, and how fast, metaluminous melts become peraluminous through reaction with these minerals, we can derive (1) an improved understanding of the speciation reactions in melt and, hence, the nature of the melt structural components, and (2) time frames for some geological processes that entail the melting of peraluminous minerals. A complementary study in progress assesses the effect of the compositional variables, in particular the activity of H_2O, on the ASI of granitic melts (e.g. London *et al.*, 2001).

In previous studies, Cooper & Kingery (1964), Samaddar *et al.* (1964) and Oishi *et al.* (1965) found that the dissolution of corundum is controlled by mass transport in the liquid phase. The experiments, however, entailed H_2O-absent ceramic systems at 1300–1600°C and 1 atm. Schairer & Bowen (1955, 1956) defined a portion of the liquidus surfaces for corundum and mullite at 1 atm in the systems $Na_2O–Al_2O_3–SiO_2$ and $K_2O–Al_2O_3–SiO_2$, and from their work the ASI of the H_2O-absent melt at corundum or mullite saturation is $\sim$1·05–1·15 for compositions closest to those of the haplogranite system. Holtz *et al.* (1992*a*, 1992*b*) and Joyce & Voigt (1994) experimentally investigated the solubility of mullite and sillimanite in the haplogranite system at elevated pressure. Although they did not provide complete details of melt compositions, their resultant glasses contained 1·9 $\pm$

0·4 to 2·3 ± 0·3 wt % normative corundum, which corresponds to ASI values of ~1·13–1·25.

The experiments reported here consist of the dissolution of corundum and andalusite into H_2O-saturated metaluminous haplogranitic liquids at 800°C and 200 MPa. Concentration profiles perpendicular to the melting interfaces are used, in conjunction with multicomponent diffusion modeling, to infer both stoichiometry and transport properties of a new set of independently diffusing components. The new set of diffusing components provide clues about species in the melt, whereas the diffusivity data allow us to estimate rates of equilibration between melt and peraluminous minerals.

MATERIALS AND METHODS

Starting materials and experimental methods

The starting materials include gem-quality single andalusite crystals from Minas Gerais, Brazil (Table 1); high-purity (99·8%) and high-density (low-porosity) alumina ceramic rods from Vesuvius–McDanel (part AXR128633004000-WJ42558) ~1·6 mm in diameter, as the corundum source; and synthetic anhydrous haplogranitic glass from Corning Lab Services, New York (Table 1), fired from reagent-grade powders at 1800°C and 1 atm to the normative composition of the haplogranite minimum at 200 MPa H_2O (Tuttle & Bowen, 1958). Andalusite and haplogranitic glass rods, ~1·7 mm in diameter and 2–5 mm in length, were prepared using a diamond core bit. Andalusite rods were cored perpendicular to the *c*-axis. Although the stable aluminosilicate phase at the experimental temperature and pressure is sillimanite, we used andalusite because we could not obtain sillimanite single crystals of sufficient purity for this purpose. Andalusite, however, showed no signs of reaction to sillimanite or mullite in these experiments. The value of ΔG for the andalusite-to-sillimanite reaction at the experimental conditions is very small [−260·06 J/mol, calculated from thermodynamic properties for andalusite and sillimanite taken from Robie *et al.* (1978) and Holdaway & Mukhopadhyay (1993)] and of the same order of magnitude as the uncertainties for the measured thermodynamic properties of both minerals. The alumina rod, consisting of an aggregate of randomly oriented corundum microlites (grain size ~20–50 μm), was cut perpendicular to its major axis in pieces ~2 mm long. Before loading, rod faces were ground flat and polished down to 0·3 μm using alumina abrasive.

Glass rods were juxtaposed against andalusite or alumina rods inside ~1·8 mm i.d. platinum capsules, with 10–15 wt % deionized and ultrafiltered water added previously to ensure that all experiments were H_2O saturated. In some runs, a small amount of gold powder (grain size ≤5 μm) was added between the rods to mark the initial position of the mineral–melt interface and hence to allow calculation of dissolution rates. We also conducted experiments consisting of an ~400 μm thick melt column sandwiched between two corundum rods. This shorter diffusion distance allowed the mineral–melt system to approach equilibrium via diffusion on a shorter time frame. Capsules were frozen before welding to prevent volatilization of added water. After welding, all capsules were heated to 100°C for 24 h to distribute H_2O and test for leaks.

Experiments were performed in cold-seal reaction vessels inclined ~15° from the horizontal. Capsules were placed with their long axes parallel to the vessels, such that the mineral–melt interfaces remained near vertical during the experiments. Runs were conducted at 800°C and 200 MPa for durations of 12–2900 h. The capsules were pressurized at room temperature, and then the temperature was raised to the experimental temperature in ~20 min. Temperature was monitored with internal chromel–alumel thermocouples, and pressure was measured with a factory-calibrated Heise bourdon tube gauge. Variations of temperature and pressure with respect to the target values during the experiments were less than 2°C and 10 bars, respectively. Total temperature and pressure uncertainties are ±4°C and <10 MPa, respectively. Oxygen fugacity was controlled by the composition of the NIMONIC 105® vessels at ~0·5 log units below the Ni–NiO buffer. Experiments were quenched using a jet of air plus water at a rate of ~75°C/min. Capsules were weighed to check for leaks and then punctured to check for H_2O saturation. Whole capsules were mounted in epoxy or Buehler Transoptic™ thermal plastic, and polished perpendicular to the mineral–glass interface until the center of the cylinders was reached. Table 2 presents a list of all the experiments, specifying starting materials, initial amount of added water, and duration.

Analytical methods

The starting anhydrous glass, andalusite, and the experimental glasses, were analyzed with a Cameca SX-50 electron microprobe at the University of Oklahoma, using an accelerating voltage of 20 kV, a beam current of 2 nA, and a 20 μm fixed spot. Sodium, potassium and aluminum were concurrently analyzed first to minimize alkali volatilization and attendant changes in elemental ratios. Counting times were 30 s on peak for all elements, yielding calculated 3σ minimum detection limits of 0·02 wt % for Na_2O, K_2O and Al_2O_3, and 0·05 wt % for SiO_2. Based on counting statistics, analytical uncertainties are in the range of 0·5–1·0% for SiO_2 and Al_2O_3, and

Table 1: Composition of the starting materials (in wt %); the anhydrous haplogranitic glass was also analyzed after hydration at 800°C and 200 MPa with different initial amounts of H_2O

Material:	Anhydrous glass		Glass + 7·5 wt % H_2O		Glass + 24 wt % H_2O		Glass + 52 wt % H_2O		Andalusite	
No. analyses:	29	SD	15	SD	15	SD	15	SD	40	SD
SiO_2	77·69	0·51	73·58	0·45	73·71	0·69	73·54	0·74	36·32	0·20
TiO_2	0·01	0·01	0·01	0·01	0·01	0·01	0·01	0·01	0·04	0·02
Al_2O_3	13·02	0·16	11·74	0·17	11·79	0·19	11·87	0·19	64·02	0·35
FeO*	0·02	0·01	0·02	0·01	0·02	0·01	0·02	0·01	0·31	0·12
MnO	0·00	0·00	0·01	0·01	0·00	0·00	0·00	0·00	0·00	0·01
MgO	0·01	0·00	0·01	0·00	0·01	0·00	0·01	0·00	0·09	0·05
ZnO	n.d.		n.d.		n.d.		n.d.		0·00	0·01
CaO	0·01	0·01	0·13	0·10	0·12	0·05	0·12	0·06	0·00	0·00
BaO	0·01	0·01	0·01	0·02	0·01	0·02	0·02	0·02	n.d.	
Na_2O	4·60	0·11	4·26	0·12	4·03	0·13	4·00	0·09	0·01	0·01
K_2O	4·78	0·09	4·64	0·12	4·49	0·10	4·52	0·13	0·00	0·00
P_2O_5	n.d.		0·04	0·02	0·04	0·03	0·06	0·03	n.d.	
F	0·03	0·03	0·01	0·02	0·02	0·02	0·03	0·04	n.d.	
Cl	0·01	0·01	0·01	0·01	0·01	0·01	0·01	0·01	n.d.	
O = F	−0·01		−0·01		−0·01		−0·01			
Total	100·18	0·53	94·46	0·53	94·25	0·59	94·20	0·65	100·79	0·51
ASI	1·020		0·957	0·02	1·007	0·02	1·015	0·02		
Moles Na/K	1·46		1·40	0·05	1·36	0·05	1·35	0·05		
Moles Al/Na	1·72		1·68	0·05	1·78	0·05	1·80	0·04		
Moles Al/K	2·52		2·34	0·06	2·43	0·05	2·43	0·06		

*Total Fe as FeO.
SD, standard deviation; n.d., not determined.

Table 2: Starting materials and duration of the conducted mineral dissolution experiments

Run no.	Starting materials*	H_2O† (wt %)	Duration (h)
CG 1	Water + Haplogranite glass rod	7·5	240
CG 2	Water + Haplogranite glass rod	24·0	240
CG 3	Water + Haplogranite glass rod	52·0	240
Acasi 185	Water + Haplogranite glass rod + Gold powder + Corundum rod	10·0	12
Acasi 186	Water + Haplogranite glass rod + Gold powder + Corundum rod	10·7	24
Acasi 199	Water + Haplogranite glass rod + Gold powder + Corundum rod	11·4	48
Acasi 184	Water + Haplogranite glass rod + Gold powder + Corundum rod	10·6	72
Acasi 182	Water + Haplogranite glass rod + Gold powder + Corundum rod	10·2	144
Acasi 177	Water + Haplogranite glass rod + Gold powder + Corundum rod	9·2	240
Acasi 175	Water + Haplogranite glass rod + Gold powder + Corundum rod	10·3	480
Acasi 111	Water + Haplogranite glass rod + Corundum rod	15·3	72
Acasi 107	Water + Haplogranite glass rod + Corundum rod	15·5	144
Acasi 85	Water + Haplogranite glass rod + Corundum rod	15·9	240
Acasi 88	Water + Haplogranite glass rod + Corundum rod	16·4	480
Acasi 87	Water + Haplogranite glass rod + Corundum rod	13·3	960
Acasi 124	Water + Haplogranite glass rod + Corundum rod	12·9	2160
Acasi 123	Water + Haplogranite glass rod + Corundum rod	10·5	2900
Acasi 183	Water + Haplogranite glass rod + Gold powder + Andalusite rod	11·6	72
Acasi 181	Water + Haplogranite glass rod + Gold powder + Andalusite rod	11·7	144
Acasi 178	Water + Haplogranite glass rod + Gold powder + Andalusite rod	11·6	240
Acasi 176	Water + Haplogranite glass rod + Gold powder + Andalusite rod	9·2	480
Acasi 110	Water + Haplogranite glass rod + Andalusite rod	16·6	72
Acasi 108	Water + Haplogranite glass rod + Andalusite rod	17·6	144
Acasi 125	Water + Haplogranite glass rod + Andalusite rod	12·3	2160
Acasi 122	Water + Haplogranite glass rod + Andalusite rod	13·0	2900
Acasi 171	Water + Corundum rod + Haplogranite powder + Corundum rod	22·6	240
Acasi 172	Water + Corundum rod + Haplogranite powder + Corundum rod	32·2	600

All the experiments were run at 800°C and 200 MPa H_2O.
*In the order in which they were loaded inside the platinum capsules.
†Proportion of water sealed inside the capsule with respect to the haplogranitic glass–powder.

1·5–3·0% for Na_2O and K_2O, relative to their reported concentrations in glass. Morgan & London (1996) demonstrated that, under these analytical conditions, the loss of sodium and grow-in of aluminum and silicon intensities during analysis are negligible and comparable with or less than the analytical uncertainties, so that no corrections are needed. Thus, we have tabulated the H_2O contents of quenched glasses based on the difference of the electron microprobe analysis (EMPA) totals from 100%. Morgan & London (1996) showed that, with the analytical conditions used here, the EMPA-difference method gives H_2O contents within 1–10% relative of those obtained with Fourier-transform IR (FTIR) spectroscopy. The maximum uncertainty for the calculated ASI values is $\pm 0{\cdot}02$. Anhydrous crystalline materials were used as standards: labradorite from the Stillwater complex (Montana) for aluminum, silicon and calcium; adularia from St. Gotthard (Switzerland) for potassium; and albite from Amelia County (Virginia) for sodium. Matrix reduction used the PAP correction algorithm (Pouchou & Pichoir, 1985).

In each experiment, three analytical transverses perpendicular to the mineral–glass interface were acquired: one at the center of the glass column and one within $\sim$300–400 μm of each edge. Three more transverses parallel to the mineral–glass interface were acquired at increasing distances of 30–100, 2000, and 3000–5000 μm. To analyze diffusion processes using mathematical models in one spatial dimension, it is important that diffusion takes place essentially along a direction perpendicular to the mineral–melt interface. We checked for this condition in two ways: (1) we studied in detail the composition of

glass within 1000 μm of the interface in the 72, 480, and 960 h experiments, by conducting closely spaced (100–200 μm) analytical transverses parallel to the interface; (2) we examined the chemical zonation of the glass located close to the interface in the 960 and 2900 h experiments by X-ray mapping.

RESULTS

Concentration profiles: uphill diffusion of alkalis and changes in ASI

Concentration isopleths

Measured distributions of oxide components in the region of glass close to the dissolution interface from the 72 and 480 h experiments show that concentration isopleths always are parallel to the interface. The 960 h experiment, however, demonstrates why a single centerline microprobe transverse is inadequate to characterize the diffusion profiles. In this experiment, the concentration isopleths curve and become perpendicular to the mineral–melt interface near one edge of the charge. X-ray images (Fig. 2) show that the curvature in the isopleths is spatially associated with empty spaces between glass and capsule, which were filled with H_2O vapor during the experiment. This experiment reveals that diffusion of aluminum through the vapor phase is much faster than through the melt volume. Our EMPA of each sample as described above ensured that diffusion from the edges of the melt column did not occur, or at least did not influence the diffusion profile measured along the centerline of the experiments.

Concentration profiles

The compositions of the experimental glasses along analytical transverses perpendicular to the mineral–glass interface are summarized in Table 3, where the experiments are sorted by the dissolving mineral and the presence or absence of gold powder at the interface. Within each category listed in Table 3, experimental time increases from top to bottom. We chose three points along the transverses to present the compositions of the glasses: at 20–30 μm, 300 μm, and away from the interface. The compositions corresponding to 'away from the interface' represent mean values of those points located beyond the aluminum diffusion profile, where the concentration profiles are nearly flat (see below).

In all experiments, the glass located close to the interface is characterized by a significant change from the starting composition; this portion of the glass will be referred to hereafter as the boundary layer. Beyond the boundary layer, the concentration profiles for all oxide components become essentially flat. Figures 3 and 4 show representative compositional profiles in the corundum

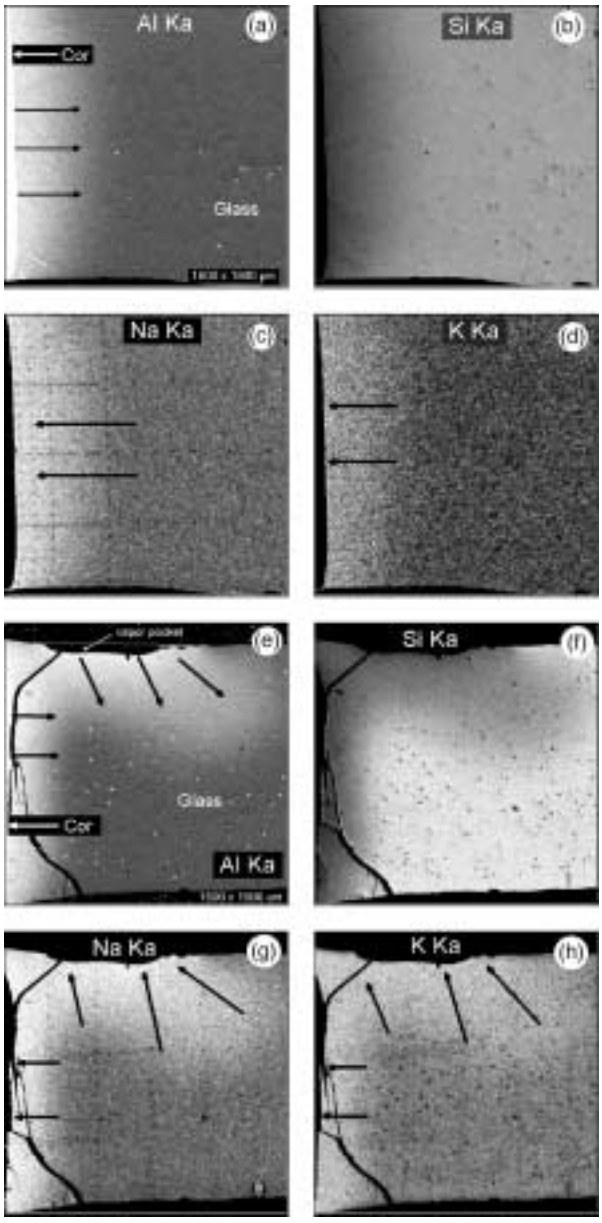

Fig. 2. X-ray maps of glasses in the 480 h (a–d), and 960 h (e–h) corundum dissolution experiments, in the region close to the corundum–glass interface. Corundum is always to the left of the glass, in white (a, e) or black (b–d, f–h). Black arrows indicate approximate directions of diffusion. White spots in (a) and (e) are vesicles filled with alumina abrasive.

dissolution experiments for three experimental times: short duration runs of 12–144 h, intermediate duration runs of 240–480 h, and long duration runs of 2160–2900 h. Comparable figures corresponding to the andalusite dissolution experiments can be downloaded from the *Journal of Petrology* web site at http://www.petrology.oupjournals.org. In all cases, the concentrations of aluminum, sodium and potassium are greatest at the

Table 3: Compositions of the experimental glasses (wt %) along analytical transverses perpendicular to the mineral–glass interface

Run no.	SiO_2	Al_2O_3	Na_2O	K_2O	H_2O*	ASI	Al/Na (mol)	Al/K (mol)	Na/K (mol)	SiO_2	Al_2O_3	Na_2O	K_2O	H_2O*	ASI	Al/Na (mol)	Al/K (mol)	Na/K (mol)	SiO_2	Al_2O_3	Na_2O	K_2O	H_2O*	ASI	Al/Na (mol)	Al/K (mol)	Na/K (mol)
	Glass composition at 30 μm from the interface									*Glass composition at 300 μm from the interface*									*Glass composition beyond the boundary layer*								
185	72·23	12·71	4·32	4·75	5·99	1·038	1·79	2·48	1·39	73·50	12·04	4·04	4·55	5·86	1·038	1·81	2·45	1·35	73·45	12·04	4·10	4·49	5·90	1·035	1·79	2·48	1·39
186	70·91	13·27	4·51	4·55	6·73	1·068	1·79	2·70	1·51	73·07	12·27	4·21	4·25	6·19	1·061	1·77	2·67	1·51	73·38	12·04	4·13	4·37	6·05	1·042	1·77	2·55	1·44
184	n.d.	n.d.	n.d.	n.d.	n.d.	n.d.	n.d.	n.d.	n.d.	73·49	11·91	3·94	4·40	6·25	1·059	1·84	2·50	1·36	73·49	11·92	4·11	4·41	6·04	1·031	1·77	2·50	1·42
182	62·40	18·09	6·42	5·20	7·79	1·105	1·71	3·21	1·88	73·16	12·12	4·05	4·31	6·33	1·067	1·82	2·60	1·43	73·18	12·17	3·98	4·39	6·26	1·075	1·86	2·56	1·38
177	64·90	17·20	5·49	5·19	7·16	1·165	1·90	3·06	1·61	73·13	12·24	3·93	4·63	6·05	1·064	1·89	2·45	1·29	73·00	12·26	3·89	4·39	6·44	1·097	1·92	2·58	1·35
175	64·80	17·13	5·55	5·04	7·36	1·157	1·88	3·14	1·68	72·72	12·14	3·79	4·22	7·10	1·120	1·95	2·66	1·36	72·96	12·02	3·86	4·36	6·77	1·082	1·90	2·55	1·35
111	65·79	17·03	5·79	5·00	6·35	1·134	1·79	3·15	1·76	73·90	11·90	4·18	4·33	5·67	1·027	1·73	2·54	1·47	73·36	11·95	4·05	4·36	6·27	1·048	1·80	2·53	1·41
107	65·99	16·50	5·79	5·04	6·63	1·095	1·73	3·02	1·75	73·16	11·87	3·95	4·36	6·66	1·058	1·83	2·52	1·38	73·22	11·98	3·98	4·36	6·44	1·060	1·83	2·54	1·39
85	65·03	17·01	5·61	5·01	7·27	1·151	1·84	3·14	1·70	73·55	12·02	3·89	4·30	6·23	1·085	1·88	2·58	1·40	73·20	12·05	3·97	4·31	6·45	1·073	1·84	2·58	1·40
88	65·30	16·93	5·29	4·87	7·51	1·200	1·94	3·21	1·65	71·67	13·04	4·32	4·37	6·59	1·100	1·84	2·75	1·50	73·58	12·03	3·86	4·31	6·20	1·090	1·89	2·58	1·36
87	65·39	16·46	5·30	4·79	8·00	1·174	1·89	3·18	1·68	72·41	12·42	3·97	4·38	6·81	1·100	1·90	2·62	1·38	73·51	11·99	3·95	4·32	6·23	1·073	1·85	2·57	1·39
124	67·21	15·44	4·54	4·75	7·99	1·211	2·07	3·00	1·45	70·04	13·60	4·08	4·60	7·61	1·148	2·02	2·73	1·35	72·27	12·09	3·65	4·29	7·65	1·128	2·02	2·60	1·29
123	68·52	15·79	4·88	4·78	5·86	1·170	1·97	3·05	1·55	69·96	14·53	4·59	4·71	6·14	1·134	1·92	2·85	1·48	73·68	12·20	3·80	4·35	5·91	1·102	1·95	2·59	1·33
183	66·36	16·49	5·76	5·22	6·13	1·084	1·74	2·92	1·68	73·73	11·97	4·00	4·45	5·82	1·045	1·82	2·49	1·37	73·73	11·97	3·95	4·39	5·95	1·061	1·84	2·52	1·37
181	65·57	16·83	5·60	5·01	6·95	1·143	1·83	3·10	1·70	73·00	12·25	3·82	4·38	6·54	1·108	1·95	2·58	1·33	73·07	12·13	3·88	4·36	6·55	1·089	1·90	2·57	1·35
178	68·48	15·23	4·88	4·86	6·52	1·141	1·90	2·90	1·53	73·95	12·08	3·93	4·24	5·80	1·092	1·87	2·63	1·41	73·63	11·98	3·86	4·33	6·19	1·085	1·89	2·56	1·35
176	67·38	15·90	5·02	4·90	6·75	1·165	1·92	3·00	1·56	73·10	12·28	3·79	4·23	6·58	1·133	1·97	2·68	1·36	72·85	12·14	3·82	4·30	6·87	1·108	1·93	2·61	1·35
110	65·87	16·37	5·33	4·98	7·44	1·155	1·87	3·04	1·63	72·88	11·96	3·79	4·41	6·95	1·084	1·92	2·50	1·31	72·84	12·12	3·89	4·37	6·77	1·087	1·89	2·56	1·35
108	67·48	15·82	5·31	4·82	6·53	1·124	1·81	3·03	1·67	72·80	11·89	4·00	4·28	7·00	1·052	1·81	2·56	1·42	73·71	11·95	3·97	4·32	6·03	1·063	1·83	2·56	1·40
125	69·09	14·40	4·51	4·70	7·27	1·147	1·94	2·83	1·46	70·33	13·51	4·07	4·49	7·60	1·170	2·02	2·78	1·38	72·48	12·07	3·74	4·29	7·41	1·116	1·96	2·60	1·33
122	68·94	14·80	4·61	4·77	6·82	1·152	1·95	2·87	1·47	70·21	13·92	4·44	4·48	6·93	1·142	1·90	2·87	1·51	73·02	12·10	3·73	4·26	6·87	1·123	1·97	2·63	1·33
	Glass composition at 30 μm from the right interface									*Glass composition at 180 μm from the right interface*									*Glass composition at 40 μm from the left interface*								
171	69·79	14·35	4·16	4·39	7·06	1·192	2·10	3·02	1·44	71·68	13·13	3·85	4·27	6·87	1·162	2·08	2·84	1·37	68·74	14·59	4·04	4·43	7·94	1·227	2·20	3·05	1·39
172	70·76	14·58	4·29	4·38	5·72	1·186	2·07	3·08	1·49	71·19	13·64	3·83	4·23	6·88	1·208	2·16	2·98	1·38	69·35	14·72	3·98	4·35	7·29	1·246	2·25	3·13	1·39

Within each group of experiments the run duration increases from top to bottom. n.d., not determined.
*Calculated by the electron microprobe analyses difference method.

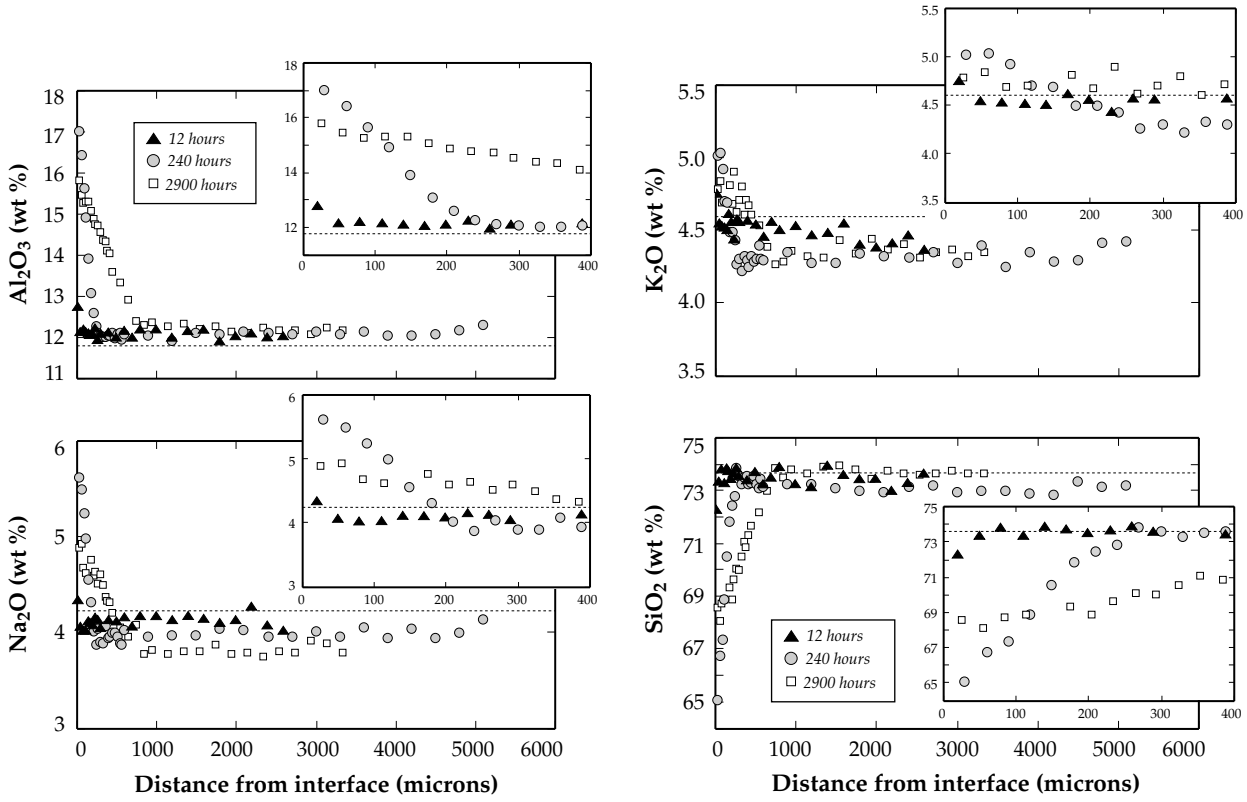

Fig. 3. Composition of glasses in the corundum dissolution experiments, as a function of experimental time and distance to the corundum–glass interface. Each concentration profile represents the mean values of three analytical transverses perpendicular to the interface. In this and following figures, the compositions are given as obtained from the microprobe, and the dashed lines refer to concentrations in the starting H_2O-saturated metaluminous melt.

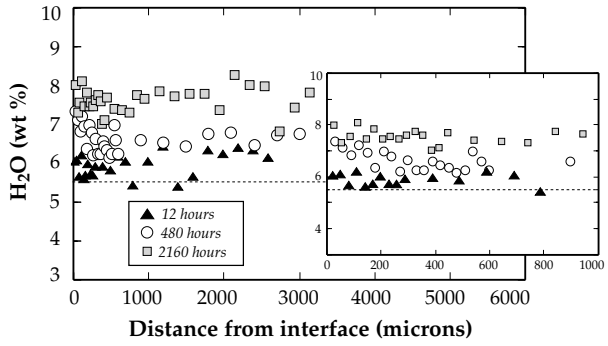

Fig. 4. Concentration of H_2O, calculated by difference of the electron microprobe analysis totals from 100%, in the corundum experimental glasses, as a function of experimental time and distance to the interface. Each concentration profile represents the mean values of three analytical transverses perpendicular to the interface.

interface and decrease away from it, whereas the concentration of silicon is least at the interface and increases away from it. Experiments of the shortest duration (12 h) yield glass cylinders that are fully and homogeneously hydrated (Fig. 5) but otherwise uniform in composition. Therefore, the melts become uniformly saturated in H_2O before any measurable diffusion of other components commences. Estimated concentration profiles for H_2O are flat for the corundum dissolution experiments of 12–144 h duration, whereas in 240–2900 h experiments H_2O increases towards the interface, matching the profiles of aluminum and alkalis.

The concentration profiles of sodium and potassium indicate that alkalis diffuse against their own concentration gradients from bulk melt through the boundary layer to the dissolution interface. Furthermore, uphill diffusion of alkalis is very rapid and affects the entire melt reservoir. This is shown by the fact that, even in experiments of only 72 h duration with glass cylinders up to 5 mm long, concentration profiles for alkalis beyond the boundary layer are flat, and the ASI of the melt increases not only at the mineral–melt interface where aluminum is being incorporated, but also throughout the entire melt column as a result of loss of alkalis via diffusion towards the interface (Table 3, Fig. 6).

At the mineral–melt interface the melt reaches an ASI of $\sim$1·20 in 480 h (Table 3, Fig. 6), and afterwards the ASI remains constant through time. The same melt ASI value of $\sim$1·20 was found by London *et al.* (2001) in

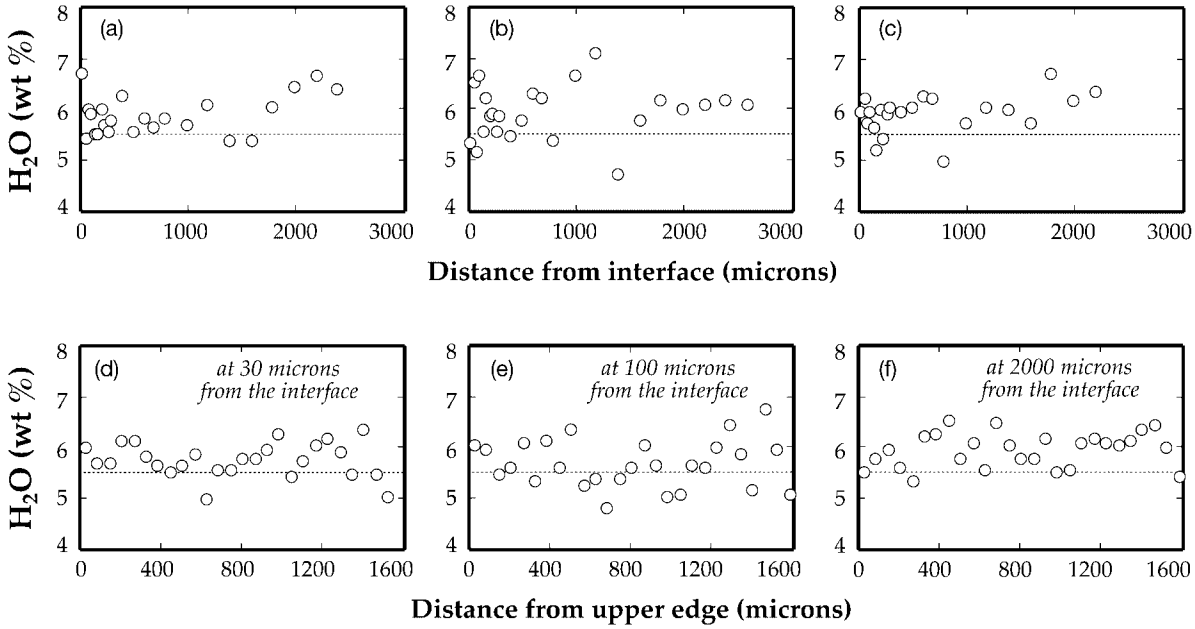

Fig. 5. H_2O concentration profiles of glasses in the 12 h corundum dissolution experiment, perpendicular (a–c) or parallel (d–f) to the interface.

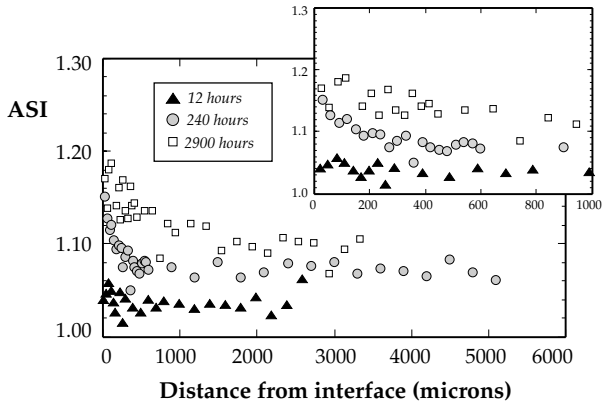

Fig. 6. ASI of glasses in the corundum dissolution experiments, as a function of experimental time and distance to the mineral–glass interface. Each profile represents the mean values of three analytical transverses perpendicular to the interface. ASI of the starting H_2O-saturated metaluminous melt is ∼1·00.

experiments in which a large fraction of corundum or andalusite was equilibrated with a small fraction of H_2O-saturated haplogranitic melt. This suggests that in these diffusion experiments with durations of 480 h or longer, the melt at the interface is in equilibrium with corundum or andalusite. Beyond the boundary layer, the ASI of the melt quickly (∼240 h) reaches a uniform value of ∼1·10 through the migration of alkalis to the boundary layer. With longer run times, the rate of increase in ASI declines and ASI increases only slightly with time up to run durations of 2900 h (Table 3).

Although Al/Si and Al/(Na + K) vary through the boundary layers as functions of position and run duration, it is notable that the molar Al/Na ratio is constant throughout the entirety of each diffusion profile; that is, the Al/Na ratio for a given experiment is the same everywhere in the melt (Fig. 7). This ratio increases steadily over the time frame of all experiments, as a result of the continuous supply of aluminum at the interface. The ratio Al/K also is uniform and increases with experimental time in the region of the melt beyond the boundary layer. Within the boundary layer, however, this ratio increases progressively towards the interface up to a maximum value of 3–3·25 (Table 3); this maximum value is reached in less than 72 h and is maintained over the time frame of all experiments. As a result, the experimental glasses are characterized by a uniform ASI throughout, except at the boundary layer where ASI increases progressively towards the mineral–melt interface.

Analysis of the ∼400 μm thick glass column sandwiched between two corundum rods along transverses perpendicular to the corundum–melt interfaces shows that the melt achieves a nearly uniform ASI of ∼1·21 (SD = 0·03) before the concentration gradients in silicon, aluminum and alkalis are erased (Table 3, Fig. 8).

Increase in melt H_2O concentration

After the metaluminous liquid becomes hydrated (in <12 h), H_2O concentration progressively increases as the melt

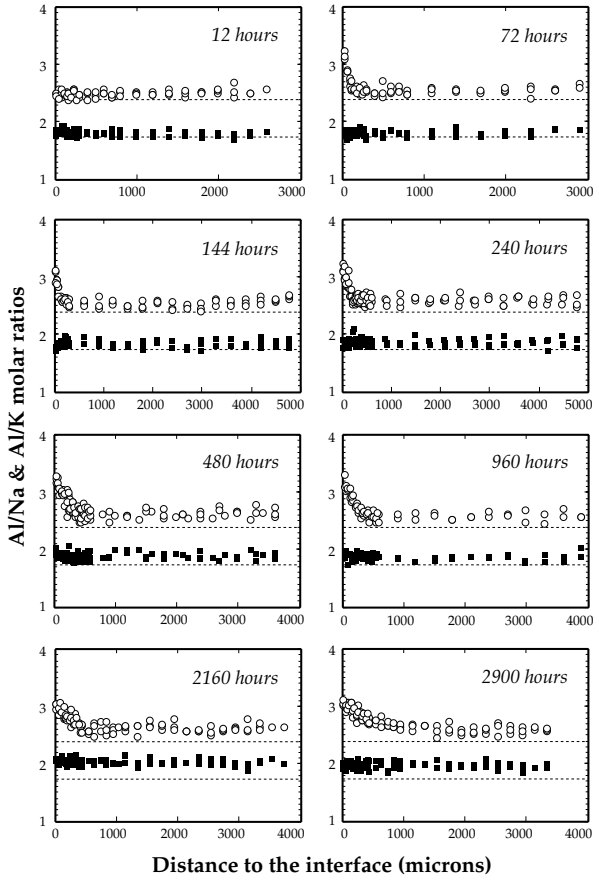

Fig. 7. Al/Na (■) and Al/K (○) molar ratios in the corundum experimental glasses along analytical transverses perpendicular to the interface.

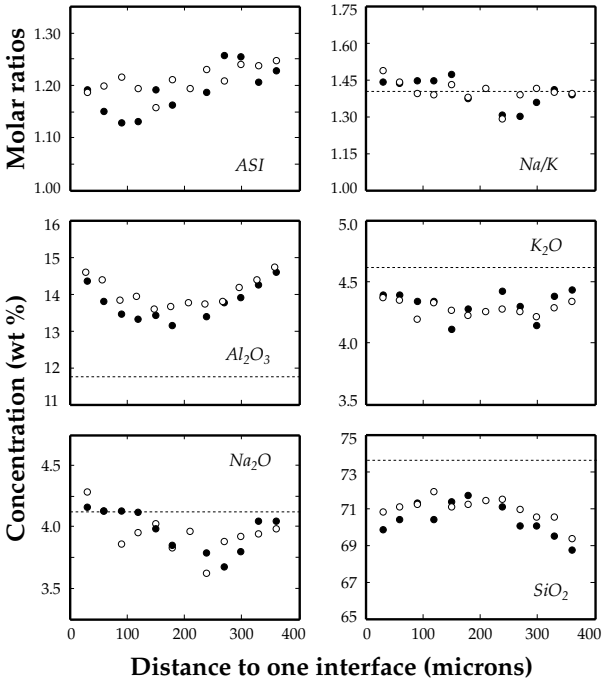

Fig. 8. Composition of glasses sandwiched between two corundum rods, along transverses perpendicular to the interfaces and after 10 (●) and 25 (○) days of experimental time. Each concentration profile represents the mean values of three analytical transverses. The distance between the two interfaces is 390–410 μm.

becomes increasingly aluminous, up to 20–30 wt % greater relative to the corresponding metaluminous melt (Table 3). This indicates that excess H_2O from the capsule is still dissolving into the melt as a result of the compositional changes taking place in the liquid as the dissolution of excess aluminum proceeds. Previous studies have already shown that H_2O solubility in granitic melts at 800–850°C and 200 MPa increases with decreasing normative quartz content and orthoclase/albite ratio (Holtz *et al.*, 1995), and limited experimental evidence shows the same correlation with increasing excess alumina (Dingwell *et al.*, 1984, 1997; Holtz *et al.*, 1992*a*; Linnen *et al.*, 1996; Behrens & Jantos, 2001). We compared the increase in H_2O solubility with excess alumina (each on a moles/100 g basis) in the experimental glasses; although the degree of correlation is low ($r = 0{\cdot}4$), in both the corundum and andalusite dissolution experiments the ratio of moles H_2O/moles excess Al_2O_3 is similar and around eight (Fig. 9a). This ratio represents the slope of a regression line obtained by minimizing the deviations of the observations from the line in both the H_2O and Al_2O_3 directions simultaneously (reduced major axis line, e.g. Davis, 1986). Scatter in the data arises in part from variations related to the calculation of H_2O by difference (discussed above), and especially because the denominator (excess Al_2O_3) approaches zero, and hence crosses the analytical detection threshold, near the metaluminous compositions that form most of the data points. These results suggest a much greater influence of excess alumina on H_2O solubility in melt than has been reported previously at these temperatures and pressures, where this ratio was found to vary between 0·1 and 1·4 (Fig. 9b). These new results, however, have to be considered with caution, as the correlation is very poor.

Composition changes at melt column boundaries

In contrast to other experimental studies on the diffusive dissolution of minerals (e.g. Zhang *et al.*, 1989; Liang, 1999), the composition of the glass at the interface and throughout the melt column is not constant through time. At the interface, concentrations achieve minimum (silicon) or maximum (aluminum, sodium, potassium) values after 72–240 h, then inverting the trends with longer run times (Table 3). Away from

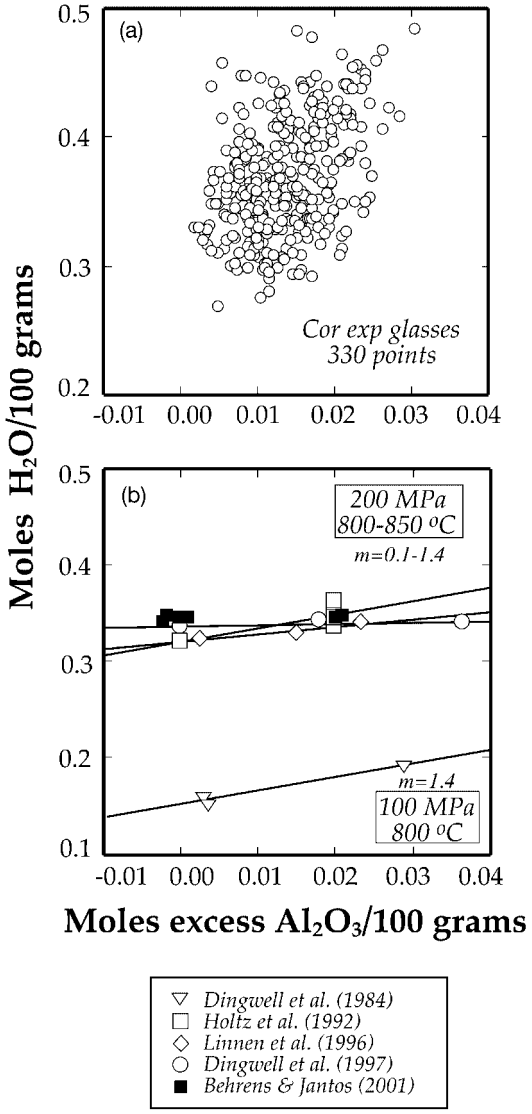

Fig. 9. H_2O vs excess Al_2O_3 concentrations in (a) glasses of the corundum dissolution experiments and (b) experimental H_2O-saturated granitic glasses reported in previous studies. *m* refers to the slope of the lines fitted to the data.

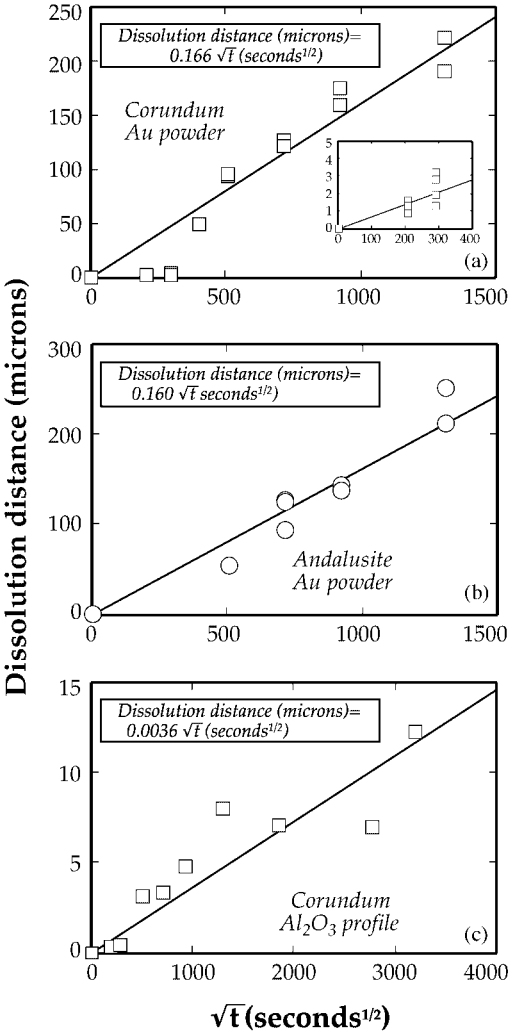

Fig. 10. Retreat of the corundum–melt and andalusite–melt interface with time, either measured with gold particles or calculated based on the alumina concentration profiles. The linear fits were forced to pass through the origin. The inset in (a) shows results from the 12 and 24 h experiments.

the interface, aluminum and H_2O increase whereas sodium and potassium decrease (Table 3). An important consequence of this behavior is that the glass does not strictly represent an infinite reservoir of the diffusing components.

Retreat of mineral–melt interface

The rate at which the corundum or andalusite interfaces retreat with melting provides information about the nature of the dissolution process (see the following section). We attempted to directly track the retreat of the interface by adding gold powder at the initial mineral–glass interface (Fig. 10a and b), and by calculations based on the final Al_2O_3/SiO_2 ratio of the experimental glass (Fig. 10c). The results show that the dissolution rates are time dependent, and the interface retreats with the square root of time. The dissolution rates measured with gold powder, however, are greater than those calculated based on the concentration profiles by a factor of 25–30. To ascertain whether the gold powder or the calculations based on the profiles give the true dissolution rate, we measured under the microscope the length of the corundum rod before and after the experiment in the 48 and 240 h runs. We found no measurable change in the length of the rod, and hence the gold powder does not

mark the original corundum–melt interface. As a final test, mass-balance calculations show that, if the distances between the gold particles and the mineral–melt interface represent corundum or andalusite dissolution distances, then the aluminum concentration in the glasses should be much higher than the measured values. We conclude that the gold particles moved away from the initial mineral–melt interface during either the experiment or quench, and that the calculations based on the chemical concentration profiles give a better approximation to the real dissolution rates.

DISCUSSION

Dissolution of corundum and andalusite in H_2O-saturated haplogranitic melts: interface reaction or diffusion in melt as rate-limiting processes

The dissolution of a mineral phase into a silicate melt that is undersaturated in all or some components of the mineral initially involves the detachment of components from the mineral surface and their incorporation in melt. Once in melt, such components can diffuse away from the mineral–melt interface with or without reaction involving components originally present in melt. Depending on the relative rates of these processes, the dissolution rate of a mineral will be limited by reaction at the interface or diffusion of components through the melt. Concentration profiles in static (non-convecting) melt, therefore, can be governed either by an interplay between interface reaction rate and diffusion, or solely by diffusion rates through the melt.

Reaction–diffusion models developed by Zhang *et al.* (1989) predict that dissolution of diopside (and possibly other silicates) becomes diffusion controlled and the melt interface composition reaches a constant or stationary saturation value in seconds. The diffusive mineral dissolution model developed by Liang (1999) predicts that the concentration profiles are independent of time when plotted against distance/time [the Boltzmann transformation discussed, for example, by Crank (1975)], and the composition of the melt at the interface is constant through time. In Liang's formulation, the composition of melt at the interface depends on only the dissolution parameter α, the initial composition of the melt and dissolving solid, and the diffusion coefficients. Both models (Zhang *et al.*, 1989; Liang, 1999) consider the melt as an infinite reservoir whose composition far away from the interface remains constant through the interval of dissolution.

The results obtained in the present experiments indicate that convection did not play a role in the redistribution of components through the melt. This is supported by the regular concentration profiles in experimental glasses, and both the increase in thicknesses of the boundary layer and decrease in the dissolution rates of the minerals with increasing experimental time [compare with, for example, Watson (1982) and Shaw (2000)]. The observed retreat of the mineral–melt interface with the square root of time (Fig. 10) suggests that diffusion in melt was the rate-limiting process. When plotted as a function of distance/$\sqrt{}$time, however, the concentration profiles do not overlap (Fig. 11). Moreover, the composition of the melt at the mineral–melt interface changes with time (Table 3).

The contrasts between our experimental results and theoretical models by Zhang *et al.* (1989) and Liang (1999) indicate that either (1) dissolution of these minerals is not controlled uniquely by diffusion in the melt, and reaction at the interface also plays a significant role, or (2) dissolution is diffusion controlled but some of the premises considered in the theoretical studies do not hold for these experiments. If the rate of the interface reaction has some effect on the kinetics of mineral dissolution, one would expect the concentration of the mineral components in the melt at the interface either to remain constant or to increase with time. This is the case for the experiments up to 72–144 h, where the concentration of aluminum increases until it reaches a maximum value (Table 3). Shaw (2000) arrived at the same interpretation of quartz dissolution experiments in basanite melt, wherein the SiO_2 concentration in the melt interface increased with experimental time. After 72–144 h, however, the concentration of aluminum in our experimental glasses at the interface decreases gradually with time. This approximately coincides with the establishment of equilibrium between the peraluminous minerals and the interface melt (see above). Although we conclude that diffusion in melt controls the concentration profiles from that point on, the change in composition at the interface and eventually throughout the entire melt column is a consequence of the finite nature of the melt reservoir together with the diffusion coupling between components derived from the dissolving mineral and melt. In the case of a finite melt reservoir, diffusion in the melt will persist until the concentration gradients for all components are erased and, therefore, those components that diffused uphill to couple with mineral components at the interface have to diffuse back towards the distant end of the melt column (Fig. 12). Because of this, the composition of the melt at the interface must change through time, and therefore the concentration profiles will not overlap when plotted against the normalized distance (distance/square root of time). The constant ASI of the interface melt at $\sim$1·20 shortly after the concentration of aluminum at the interface reaches a maximum value suggests that, from this point on, the composition of the boundary layer at the interface does lie along the corundum or

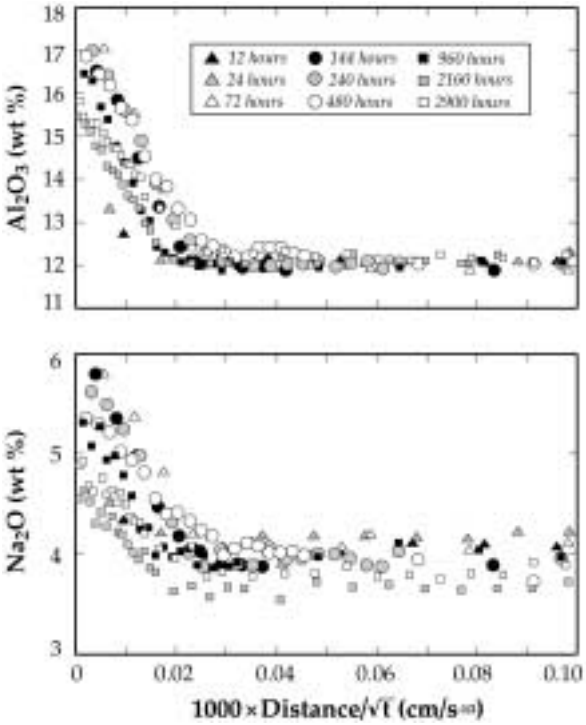

Fig. 11. Concentration of Al_2O_3 and Na_2O vs distance to the mineral–glass interface normalized to the square root of time, in glasses of the corundum dissolution experiments.

andalusite saturation surface. Changes in composition follow from migration along that liquidus surface to the bulk composition where the tie line between the initial melt composition and corundum or andalusite crosses the liquidus surface for the relevant mineral.

We suggest that the previous mineral dissolution experimental studies (Zhang *et al.*, 1989; Liang, 1999) were quenched before the limiting nature of the melt column length could influence the final development of the diffusion profile. Otherwise, the previous experiments are similar to those conducted here, wherein the boundary layer created by bi-directional diffusion of components would be erased over time, the composition at the mineral–melt interface would change over time, and the compositional profiles would become flat throughout the melt as the mineral and melt achieved chemical equilibrium. Short-duration mineral dissolution experiments are convenient tools for the extraction of diffusivities using analytical solutions for semi-infinite melt reservoirs, and only in those cases where uphill diffusion affects only that melt located close to the boundary layer, developing local troughs and humps in the concentration profiles (Fig. 13a). In cases like ours, however, where uphill diffusion involves migration along the entire melt column (Fig. 13b), information about the eigenvectors controlling the uphill diffusion will not be recovered with short-duration mineral dissolution experiments; it will only be recovered precisely with long-time diffusion experiments using analytical solutions for finite-melt reservoirs.

Multicomponent diffusion

As the dissolution of corundum and andalusite into H_2O-saturated haplogranitic melts seems to be a diffusion-controlled process at least in medium- to long-duration experiments, an understanding of the equilibration between crystals and melt requires an assessment of the multicomponent nature of diffusion in this system. The macroscopic quantitative treatment of chemical diffusion in multicomponent systems involves expressing the fluxes and concentrations of the diffusing components by $N - 1$ partial differential equations such as (1) and (2), respectively, with N being the number of chemical components in the system; these equations arise from mass conservation and a linear force-flux phenomenology (Fick's law, e.g. Crank, 1975):

$$\mathcal{J}_i = -D_{ij} \nabla C_j \tag{1}$$

$$\frac{\partial C_i}{\partial t} = \nabla \left(\sum_{j=1}^{N-1} D_{ij} \nabla C_j \right) \tag{2}$$

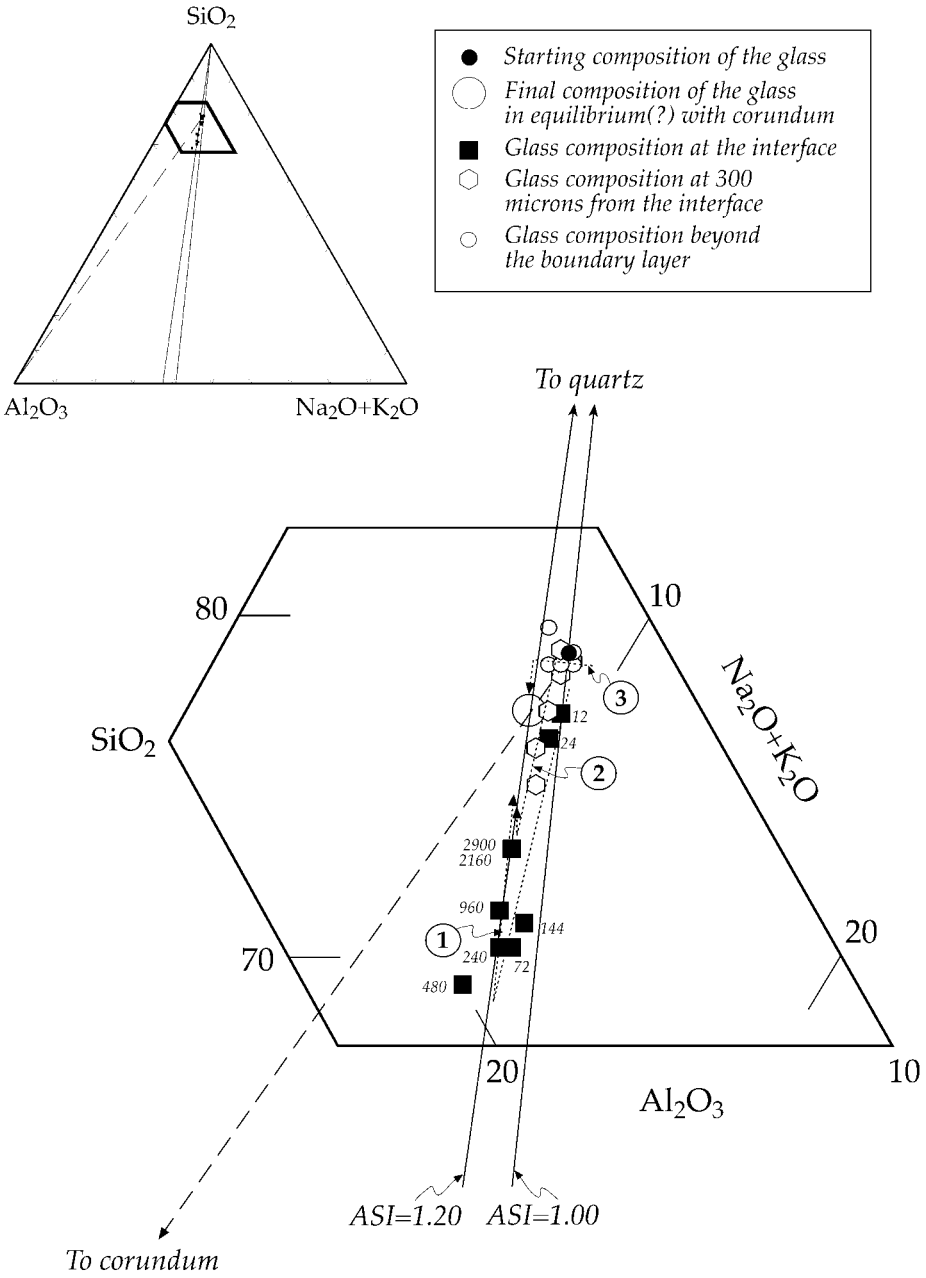

Fig. 12. Evolution of the composition of the glass through time in the corundum dissolution experiments, at the interface (1), at 300 μm from the interface (2), and beyond the boundary layer (3). The small numbers in italics refer to the duration of the experiments (only shown for the interface composition). Trajectory 1 shows how those components initially concentrated at the interface (aluminum and alkalis) diffuse back to the distant melt, with the composition of the interface melt tending towards the intercept between the 1·20 ASI line and the tie line joining initial melt and corundum. The constant ASI of the melt at ~1·20 after 480 h suggests that the changes in composition from that point on follow from migration along the corundum liquidus surface. Trajectory 1 is initially dominated by the incorporation of aluminum from corundum and alkalis from the distant melt through v_{Na} and v_K, and later by the migration of aluminum and alkalis towards the distant melt through v_{Al}. Trajectory 3 is due to the loss of alkalis to the interface through v_{Na} and v_K. Trajectory 2 is controlled for a short time by the loss of alkalis to the interface, and then by the arrival of aluminum and alkalis from the interface through v_{Al}. Although these experiments did not last long enough to observe the final stages of equilibration, we postulate that trajectories 2 and 3 would end as trajectory 1, turning towards the intersection between the 1·20 ASI line and the tie line joining initial melt and corundum, once the melt reaches an ASI of 1·20. From that point on, all the trajectories (compositional changes in the melt) would be controlled by the migration of aluminum and alkalis through v_{Al}. In that way, the melt would erase the concentration gradients while maintaining the 1·20 equilibrium ASI.

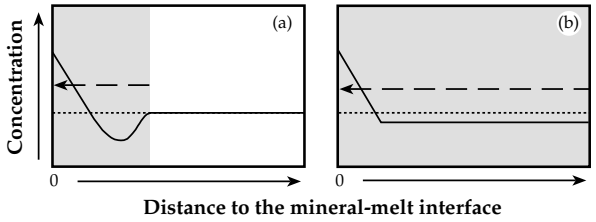

Fig. 13. Two contrasting cases of uphill diffusion, involving either the melt region close to the boundary layer (a) or the entire melt reservoir (b). Dotted line indicates initial concentration of a given component in melt, and continuous line shows the concentration of this component after uphill diffusion. Shaded areas and dashed arrows indicate the melt region and direction, respectively, in which uphill diffusion takes place.

where $\mathcal{J}_i$ and C_i refer to the flux and concentration of component i, respectively, t refers to time, and ∇C_j is the concentration gradient of component j. The flux and concentration of the Nth component is fixed by those of the other components through closure. D_{ij} is the diffusion coefficient expressing the proportionality between the flux of component i and the concentration gradient of component j. The complete set of diffusion coefficients relating fluxes and concentration gradients, arranged in columns and rows, constitute the diffusion matrix [D] that characterizes the transport properties of the system. In a system with N components, [D] will be an $N - 1$ by $N - 1$ matrix. Diffusion coefficients relating the flux of a component to its own concentration gradient (D_{ij}, where $i = j$) are referred to as diagonal terms of the diffusion matrix; those relating the flux of a component to the concentration gradient of other component (D_{ij}, where $i \neq j$) are referred to as off-diagonal terms. The matrix [D], however, is not unique for a given system at any given conditions; it is only specific to the choice of solvent (the Nth component) and the chosen set of diffusing components and their stoichiometries (e.g. Zhang, 1993; Chakraborty, 1995; Liang *et al.*, 1996; Mungall *et al.*, 1998).

Previous diffusion studies in silicate melts have already shown that the fluxes of the arbitrarily chosen oxide components (i.e. SiO_2, Al_2O_3, etc.) rarely are independent of each other (e.g. Oishi *et al.*, 1965; Cooper & Schut, 1980; Zhang *et al.*, 1989; Wolf & London, 1994; Chakraborty *et al.*, 1995*a*; Liang *et al.*, 1996; Mungall *et al.*, 1998; Shaw, 2000). Instead, they are coupled through the off-diagonal terms of the associated diffusion matrix [D]. A method of determining the stoichiometries of the components that diffuse independently of each other, along with values of their diffusivities, consists of finding the eigenvectors (v_i) and eigenvalues (λ_i) of the matrix [D] associated with the oxide components (e.g. Trial & Spera, 1994; Chakraborty, 1995; Mungall *et al.*, 1998). The eigenvectors represent these 'new' diffusing components expressed as linear combinations of the 'old' oxide components; the eigenvalues correspond to the diffusion coefficients of these independent diffusing components. The eigenvectors, therefore, can be viewed as a new set of chemical components that have the virtue of uncouple chemical diffusion, meaning that the fluxes of these components proceeds independently of each other. Thus, in an N-component system, there will be $N - 1$ independent eigenvectors, and $N - 1$ eigenvalues. The orientation of the eigenvectors in composition space as well as the eigenvalues for a system at some given temperature and pressure conditions are independent of the choice of solvent or components and, therefore, are invariant properties of the system (e.g. Chakraborty *et al.*, 1995*b*, and references therein; Liang *et al.*, 1996; Mungall *et al.*, 1998). The orientation of each eigenvector is given by $N - 1$ associated coefficients that express the relationships with respect to the oxide component reference frame. As the relative values of the $N - 1$ coefficients for each eigenvector are constant, the value of one of them can be fixed to be a constant number, e.g. unity. The arrangement of the eigenvector coefficients in columns results in another $N - 1$ by $N - 1$ matrix, [P]. Thus, P_{ij} are coefficients of the [P] matrix and measure the participation of the oxide component i on the eigenvector v_j.

The nature of the independent diffusing components is investigated through diagonalization of [D]. As the diffusion matrix [D], however, is not known *a priori* for a given system and conditions, eigenvectors and eigenvalues have to be obtained from the oxide concentration profiles measured in the experimental glasses. That leads to a new set of $N - 1$ uncoupled partial differential diffusion equations, equivalent to (2), each of them expressing now the change in concentration of an independent diffusing component (v_i) with time as a function of its concentration gradient and its diffusion coefficient (λ_i):

$$\frac{\partial C_{v_i}}{\partial t} = \nabla (\lambda_i \nabla C_{v_i}) \qquad (3)$$

here C_{v_i} refers to the concentration of the eigenvector v_i. These partial differential equations have to be solved with appropriate boundary and initial conditions, and the analytical solutions are then used to obtain eigenvectors and eigenvalues through a forward-modeling approach in which the differences between calculated and experimental concentration–distance–time data are minimized iteratively (Mungall *et al.*, 1998). The function used to quantify such differences is the χ^2 function (see Trial & Spera, 1994; Mungall *et al.*, 1998). Thus, according to the multicomponent diffusion model and using 6-oxygen molecular stoichiometry for the oxide components and Si_3O_6 as the solvent, the equation relating the concentration of Al_4O_6 to the eigenvectors and

eigenvalues is the following (e.g. Zhang *et al.*, 1989; Mungall *et al.*, 1998):

$$C_{Al_4O_6\{x,t\}} = C_{Al_4O_6\{\infty\}} + P_{AlAl}C_{v_{Al}}P^{-1}_{AlAl}(C_{Al_4O_6\{o\}} - C_{Al_4O_6\{\infty\}}) + P_{AlNa}C_{v_{Na}}P^{-1}_{NaNa}(C_{Na_{12}O_6\{o\}} - C_{Na_{12}O_6\{\infty\}}) + P_{AlK}C_{v_K}P^{-1}_{KK}(C_{K_{12}O_6\{o\}} - C_{K_{12}O_6\{\infty\}}) + P_{AlH}C_{v_H}P^{-1}_{HH}(C_{H_{12}O_6\{o\}} - C_{H_{12}O_6\{\infty\}}) \quad (4)$$

where $C_{i\,(x,t)}$ is the concentration of i at distance x from the interface and at time t, $C_{i\,(\infty)}$ refers to the initial concentration of component i, $C_{i(o)}$ is the concentration of component i at the interface, P_{ij} are coefficients of the $[P]$ matrix, $P^{-1}{}_{ij}$ are coefficients of the inverse $[P]$ matrix, and C_{vj} expresses the concentration of the eigenvector v_j at the given time and distance and for a given eigenvalue λ_j.

The method described above, however, requires rigorous multivariate curve fitting techniques, and in our case does not yield unique results. This is due to the large number of unknown parameters: in the five-component system under investigation here, there are 16 unknowns—three coefficients for each of the four eigenvectors, plus four associated eigenvalues. Moreover, the mineral and melt compositions we used cover only one direction in compositional space, as the angle between the vectors corundum–melt and andalusite–melt is small. Trial & Spera (1994) showed that, for the magnitude of the uncertainties associated with electron microprobe analyses, it is possible to recover only some of the elements of the diffusion matrix from multiple (time series) experiments involving a single direction in composition space. Furthermore, that direction should not coincide with any eigenvector (Trial & Spera, 1994), or lie within a plane that contains two eigenvectors with associated eigenvalues of the same magnitude within measurement error (Mungall *et al.*, 1998). Following Liang *et al.* (1996), an accurate estimate of the diffusion matrix in an $\mathcal{N}$-component system requires diffusion experiments along at least $\mathcal{N} - 1$ directions in composition space that cross at a given composition (that of interest) and are orthogonal to each other.

Despite these restrictions inherent to the system of interest here, in the next section we show how the concentration profiles and elemental covariations obtained from the dissolution of corundum or andalusite in H_2O-saturated haplogranitic melt bear important information about transport properties in this system, specifically about the diffusing component controlling the migration of aluminum through the melt.

Analysis of concentration profiles: observations on relative component motion

Dissolution of corundum or andalusite into H_2O-saturated haplogranitic melt does not simply consist of surface detachment and diffusion of the 'quasicrystalline' mineral components away from the mineral–melt interface, but involves the uphill diffusion of alkalis (Fig. 3). That guarantees that the direction in compositional space defined by corundum–melt or andalusite–melt pairs does not coincide with any eigenvector. Moreover, although the length scale of diffusion for all the oxide components might appear similar, the initial concentrations of alkalis change throughout the entire melt column well above the uncertainties associated with the microprobe analyses. This indicates that diffusion profiles are not binary and, therefore, that mineral–melt directions do not lie within a plane containing two eigenvectors with associated eigenvalues of the same magnitude.

In previous studies, uphill diffusion of alkalis and, in general, any other component in the melt, has been explained either by changes in activity coefficients with melt composition (e.g. Sato, 1975; Watson, 1982; Chekhmir & Epel'baum, 1991; Lesher, 1994; Shaw *et al.*, 1998; Shaw, 1999) or as the result of coupled diffusion in multicomponent systems (Zhang *et al.*, 1989; Chakraborty, 1995; Chakraborty *et al.*, 1995*a*; Liang *et al.*, 1996; Mungall *et al.*, 1998, and references therein). The diffusion matrix $[D]$ can be expressed as the product of two other matrices, $[L]$ and $[G]$. The kinetic matrix $[L]$ measures the effect of intrinsic mobilities and concentrations on the flux of diffusing components; the thermodynamic matrix $[G]$ expresses the dependence of fluxes on the variation of chemical potentials—and therefore activity coefficients—with composition (e.g. Liang *et al.*, 1997). Thus, the off-diagonal terms of $[D]$ being different from zero, and therefore diffusion coupling, can be due to $[L]$, $[G]$, or both (e.g. Chakraborty *et al.*, 1995*a*; Liang *et al.*, 1996).

In the experiments presented here alkalis concentrate at the boundary layer, the region of the melt with the lowest silica and highest alumina concentrations. The local coordination of excess alumina in granitic melts is not yet clear (e.g. Lacy, 1963; Mysen *et al.*, 1981*b*; Sato *et al.*, 1991; Poe *et al.*, 1992). Thus it is not obvious if the boundary layer melt is more or less polymerized than the distant melt, and therefore it is not clear if uphill diffusion of alkalis is due to partitioning between contacting melts as proposed by Watson (1982). The fact, however, that the flux of sodium through the melt is such that the molar Al/Na ratio is constant in the entire melt reservoir indicates that sodium (and possibly potassium) diffuses uphill in response to the flux of aluminum. It strongly suggests also that coupled diffusion is driven by the kinetic matrix $[L]$, and that either aluminum and sodium activity coefficients do not vary with melt composition for the range of compositions found in our experiments, or they vary proportionally and in the same direction.

We propose, therefore, that an aluminum–alkali component may approximate one of the eigenvectors (v_{Al}) in this system at the temperature and pressure investigated. Diffusion along that direction in composition space would be responsible for the migration of aluminum and alkalis away from the interface in these experiments. The proportion of aluminum to sodium in this component is necessarily fixed by the aluminum to sodium ratio in the bulk melt, as shown in Fig. 7. That requires that this ratio will depend on the composition of the melt. The proportion of aluminum to potassium is such as to maintain an aluminum to total alkali molar ratio at $\sim$1·20, which is the ASI of an H_2O-saturated haplogranitic melt in equilibrium with corundum or andalusite at the experimental temperature and pressure (London *et al.*, 2001). This interpretation is suggested by experiments 171 and 172 (Table 3), in which the melt achieved a nearly uniform ASI of $\sim$1·20 before the concentration gradients in the oxide components were erased. As this is the equilibrium ASI of the melt, it is not likely to change from that point on during the redistribution of aluminum and alkalis through v_{Al}, implying that the direction of this eigenvector is along a constant ASI of 1·20.

Our results do not suggest any coupling of silicon with the rest of the oxide components. To test this, we compared analyzed silica concentrations in the 480 and 2900 h corundum dissolution experiments with theoretical values, calculated assuming that silica concentration is determined only by the migration of the other components. The theoretical concentrations are very close to the analytical values, suggesting to us that P_{SiAl}, P_{SiNa}, P_{SiK}, and P_{SiH} coefficients are close to zero, and that diffusion along the direction of the silicon eigenvector (v_{Si}) is much slower than along the directions of the other eigenvectors in the system; that is, $\lambda_{Si} < \lambda_{Na}$, λ_K, λ_{Al}, and λ_H. This is not surprising, as in previous diffusion studies silica has always been found to constitute one of the slowest diffusing components (e.g. Watson, 1982; Baker, 1990). Our data, however, do not permit us to obtain the stoichiometry of v_{Si}.

Sodium and potassium diffuse through the bulk melt, faster than, and independently of, aluminum and silicon. This is indicated by the uphill diffusion of sodium and potassium towards the interface, the commensurate drop in their oxide concentrations in the glass beyond the boundary layer, between 7 and 12 wt % relative (Tables 1 and 3), and the small changes in the concentrations of alumina and silica beyond the boundary layer, between 1 and 3 wt %. In the case of alumina, the small increase in its concentration away from the interface can be explained by the migration of alkalis; in the case of silica, the changes are erratic but still very small. On the other hand, preliminary results of albite and K-feldspar dissolution experiments with the same starting glass and experimental conditions indicate that the fluxes of sodium and potassium are uncoupled (Acosta *et al.*, 2000). We conclude that sodium and potassium, alone or with some exchange involving hydrogen (see below), may represent two directions in composition space along which diffusion is uncoupled, v_{Na} and v_K, respectively. Uphill diffusion of alkalis towards the interface would be accomplished along these directions.

The rapid hydration of the glasses without any noticeable diffusion of other components suggests that the eigenvector controlling the diffusion of hydrogen, v_H, is parallel to the H_2O axis, and that the associated eigenvalue is one of the largest of the system. Our data also indicate that hydrogen might be coupled with other components. H_2O concentration profiles, which generally increase towards the interface and match alumina profiles in the corundum experiments, give the appearance of uphill diffusion of this component and suggest coupling with aluminum. The increase in H_2O solubility with excess aluminum in the melt may indicate that excess aluminum associates with H_2O or its components in the melt and hence reduces its activity (e.g. London *et al.*, 2001). We propose that some of the dissolved H_2O dissociates to provide charge balance for the excess aluminum entering the melt that is not balanced by alkalis, and for the excess alumina created in the bulk melt that experiences alkali loss via diffusion. The H_2O concentration profiles, therefore, could be the result of diffusion along more than one direction in composition space. The high uncertainty associated with H_2O concentrations, however, does not permit us to infer the stoichiometry of H_2O in these eigenvectors.

Extraction of diffusivities

The only component for which diffusivity can be assessed from these experiments is the aluminum–alkali component. Silica concentration profiles are dominated by diffusion of the rest of components, which provides only an upper limit for its diffusivity. In addition, although accomplished by diffusion along the sodium and potassium eigenvectors, uphill migration of alkalis is driven by the incorporation of aluminum into the melt at the interface; this provides only a minimum value for these diffusivities.

Diffusion along the direction of the aluminum–alkali eigenvector, however, will arguably control the equilibration between H_2O-saturated haplogranitic melts and peraluminous minerals and, therefore, the diffusion coefficient or eigenvalue associated with this eigenvector will provide information about the kinetics of this equilibration. We calculated this diffusivity in two ways. First, we applied a multicomponent diffusion model using the forward-modeling approach described in the multicomponent diffusion section. Second, we calculated

the effective binary diffusion coefficient (Cooper, 1968) associated with Al_2O_3.

Multicomponent diffusion modeling

The ideal analytical solution to the uncoupled differential diffusion equations that apply to our experimental results should be one taking into account the following: (1) the melt represents a finite reservoir; (2) the melt composition at the interface changes with time along the corundum–andalusite liquidus surface of the system; (3) the mineral–melt interface is not fixed but retreats with a velocity that is a function of time. None of the existing published solutions for mineral dissolution via diffusive transport, however, meet all of these conditions. As an approximation, we apply here two available solutions. First, one in which the melt reservoir is considered a semi-infinite medium, the mineral–melt interface is fixed, and the composition of the melt at the interface is constant through time (Crank, 1975):

$$C_{v_j\{x,t\}} = C_{v_j\{o\}} \operatorname{erfc} \frac{x}{2\sqrt{\lambda_j t}} \quad (5)$$

where $C_{v_j\{x\,t\}}$ is the concentration of the eigenvector v_j at distance x from the interface and at time t, $C_{v_j\{o\}}$ is the concentration of v_j at the interface, and erfc $\{x\}$ refers to the complementary error function (= 1 − erf $\{x\}$). The second solution, taken from Smith *et al.* (1955), takes into account that the mineral–melt interface retreats, although at a constant velocity V:

$$C_{v_j\{x,t\}} = C_{v_j\{\infty\}} + \frac{C_{v_j\{o\}} - C_{v_j\{\infty\}}}{2} \exp[-(Vx)/\lambda_j] \operatorname{erfc} \frac{x - Vt}{2\sqrt{\lambda_j t}} - \frac{C_{v_j\{o\}} - C_{v_j\{\infty\}}}{2} \operatorname{erfc} \frac{x + Vt}{2\sqrt{\lambda_j t}}. \quad (6)$$

$C_{v_j\{\infty\}}$ refers to the initial concentration of v_j. Both of these solutions also assume that diffusion takes place only in one direction in space, that the diffusion coefficients do not change with the composition of the melt, and that the changes in the density of the melt with composition are negligible. We checked the first assumption with closely spaced analytical transverses and the X-ray raster mapping. The third assumption was checked by calculation of the melt densities along the analytical transverses perpendicular to the interface. Densities within the boundary layer are equal to or up to 0·05 g/cm^3 higher than those beyond the boundary layer, ~2·27 g/cm^3; we used for these calculations data from Lange & Carmichael (1990), Silver *et al.* (1990) and Richet *et al.* (2000).

For both solutions we calculate the eigenvalue associated with the aluminum–alkali eigenvector for every experimental time equal to or greater than 240 h, using the composition of the melt at the interface at that time as the constant interface value, and the mean composition of the melt beyond the boundary layer as the starting melt composition. As in our experiments the mineral–melt interface retreats with the square root of time, the velocity of retreat at every experimental time is taken as the slope of the tangent to the function fitted to the experimental data at that time. To compare our results with previous ones we choose 6-oxygen molecular stoichiometry for the oxide components, Al_4O_6, $Na_{12}O_6$, $K_{12}O_6$, and $H_{12}O_6$, with Si_3O_6 as the solvent. According to the discussion in the previous section, some of the eigenvector coefficients are fixed (Table 4), and the only coefficients we let vary during the modeling are P_{Hj} and P_{iH}. A Levenberg–Marquardt algorithm was used to calculate iteratively χ^2 for different sets of eigenvectors and diffusion coefficients until the χ^2 value was lower than an established threshold.

Table 4: Eigenvectors (v_i) coefficients deduced from analysis of the concentration profiles and referred to 6-oxygen oxide components with Si_3O_6 as solvent

	v_{Al}	v_{Na}	v_K	v_H
Al_4O_6	1	0	0	?
$Na_{12}O_6$	0·186, 0·170	1	0	?
$K_{12}O_6$	0·092, 0·107	0	1	?
$H_{12}O_6$	?	?	?	1

The diffusion coefficients for v_{Al} obtained with both solutions, together with the associated χ^2 values, are presented in Table 5. Figure 14 shows the fit obtained for the 2900 h experimental data. The main conclusions drawn from that modeling are the following. The best fits (lower χ^2 values) are always obtained when the eigenvalue for v_{Al} is around $1{\cdot}0 \times 10^{-10}$ cm^2/s, independently of the values of P_{Hj} and P_{iH}. The values found for this eigenvalue with both solutions and for all the experimental times are relatively close, so that the lowest and highest values are different by a factor of six. This observation supports our interpretation that mineral dissolution is diffusion controlled, at least after 240 h. Different sets of values for P_{Hj} and P_{iH} yield adequate fits to the concentration profiles and, therefore, we cannot extract any unique information about diffusion of water from these experiments. The eigenvalues obtained for the rest of the eigenvectors are always similar to that for v_{Al}, reflecting that concentration profiles are mostly controlled by diffusion along the v_{Al} direction. They are not reported here as we think they are inaccurate representations of component diffusivities (as a result of system restrictions discussed above).

Table 5: Eigenvalues calculated for v_{Al} with two different solutions [Smith et al. *(1955) and Crank (1975)] and effective binary diffusion coefficient (EBDC) calculated for Al_2O_3 with Crank (1975) solution*

Run duration (h)	Dissolution rate ($\times 10^{-10}$ cm/s)	v_{Al}, Smith *et al.* (1955)		v_{Al}, Crank (1975)		EBDC, Crank (1975)	
		($\times 10^{-10}$ cm^2/s)	χ^2	($\times 10^{-10}$ cm^2/s)	χ^2	($\times 10^{-9}$ cm^2/s)	r
240	2·203	1·4	0·011	1·4	0·011	1·5	0·99
480	1·125	1·9	0·012	1·8	0·012	2·1	0·94
960	0·548	0·3	0·003	0·3	0·004	1·0	0·99
2160	0·255	0·9	0·007	0·9	0·007	2·0	0·98
2900	0·193	1·4	0·009	1·4	0·009	3·6	0·97

The goodness of the fit between model and experimental data is shown by the χ^2 function and the correlation coefficient r.

Effective binary diffusion coefficients (EBDC)

Cooper (1968) showed that diffusion in multicomponent systems can be treated as pseudobinary through the concept of EBDC; that is, each component can be thought of as the solute and the rest of components represent the solvent. That requires that the system is semi-infinite with respect to diffusion and that concentration profiles have no extrema. The EBDC for a component i ($D_{i(EB)}$) and its relationship with [D] are given by the following equations (Cooper, 1968; Chakraborty & Ganguly, 1992):

$$\mathcal{J}_i = -D_{i(EB)}\frac{\partial C_i}{\partial x} \tag{7}$$

and

$$D_{i(EB)} = D_{ii} + \sum_{j=1}^{j=n-1} D_{ij}{}_{j\neq 1}\frac{\partial C_j}{\partial C_i}. \tag{8}$$

The calculation of the EBDC for a given component in a multicomponent system using experimental diffusion data involves fitting the concentration profile of that component with the appropriate analytical solution of the differential diffusion equation, and obtaining a diffusivity value from that fit. A good fit between experimental and theoretical concentrations does not mean, however, that the EBDC can describe the diffusive transport in that system at the given temperature and pressure conditions. That would be true only in two cases: (1) diffusion coupling between components is negligible, with vanishingly small off-diagonal terms in the diffusion matrix (in this case the EBDC would coincide with the diagonal terms of [D]); or (2) the concentration gradients to be modeled ($\partial C_j/\partial C_i$) are similar to those in the experiments where the EBDC were measured (Chakraborty & Ganguly, 1992; Chakraborty, 1995; Chakraborty *et al.*, 1995*a*).

For the experiments presented in this paper, it is not appropriate to calculate EBDC for SiO_2, Na_2O or K_2O, because their concentration profiles seem to be largely controlled by the diffusion of aluminum. It is potentially useful to calculate an EBDC for Al_2O_3 because, in natural systems, the dissolution of peraluminous minerals in hydrous granitic melts at ~800°C and low pressures would take place along the same direction in compositional space and, therefore, will impose concentration gradients in melt similar to those obtained in our experiments. $D_{Al_2O_3(EB)}$ can then be used to estimate the time needed for equilibration between peraluminous minerals and H_2O-saturated granitic melts, provided that the saturation values of the peraluminous minerals in melt are known. The effects of other usual major components in natural melts such as Ca, Fe and Mg may have to be taken into account (e.g. see Liang *et al.*, 1996), but the concentrations of these components are low in synthetic liquids representative of peraluminous S-type granitic melts (e.g. London, 2001).

Table 5 shows calculated $D_{Al_2O_3(EB)}$ for every experimental time, using the Crank (1975) solution. The fits to the experimental data are good (Fig. 15) and diffusion coefficients, $\sim 2{\cdot}0 \times 10^{-9}$ cm^2/s, are again similar for experimental times ranging from 240 to 2900 h. $D_{Al_2O_3(EB)}$ is, however, about 10–30 times higher compared with the eigenvalue calculated for v_{Al}. This disparity could result from coupling of aluminum with some of the other components [see equation (4)].

Melt species and the stoichiometry of the eigenvectors

The orientation of the eigenvectors in compositional space, a fundamental property of the system at fixed temperature and pressure conditions, is given by the

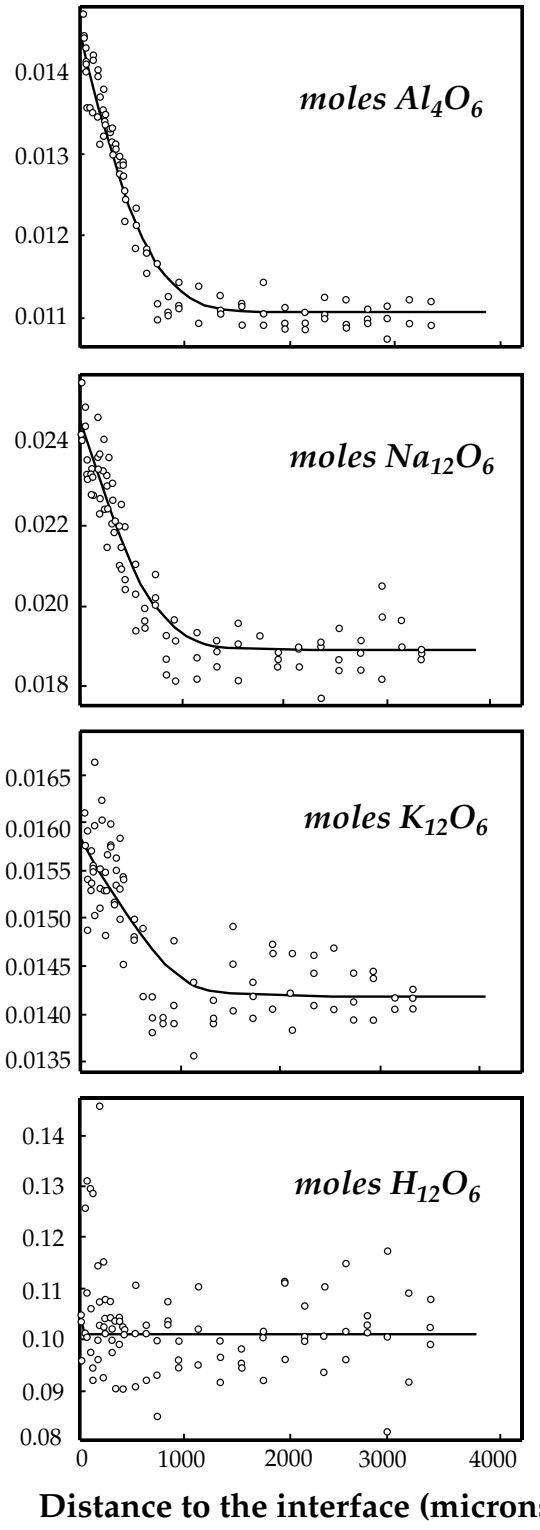

Fig. 14. Example of fits obtained from the multicomponent diffusion modeling for the 2900 h corundum dissolution experimental data, using the solution provided by Smith *et al.* (1955).

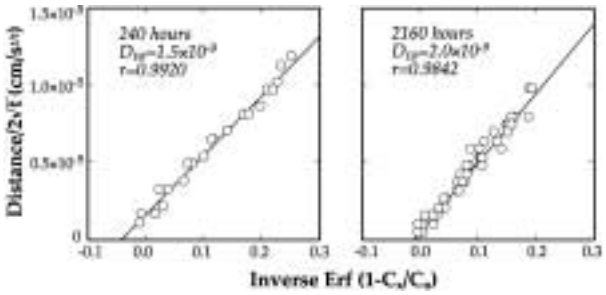

Fig. 15. Examples of calculated effective binary diffusion coefficients (D_{EB}) for alumina using Al_2O_3 concentration profiles from the corundum dissolution experiments. The diffusion coefficient corresponds to the square of the slope of the linear fit.

coefficients of the matrix [*P*]. These coefficients express the proportions among the oxide components of the system for each of the eigenvectors. Eigenvectors uncouple chemical diffusion, and hence they reflect the homogeneous reactions taking place in the liquid during diffusion to minimize its free energy. Do the eigenvectors contain information on the stoichiometry of chemical species present in the melt? Chakraborty *et al.* (1995*b*) regarded the stoichiometry of the exchange reactions taking place in the melt, which can be calculated from the eigenvector coefficients, as equivalent to the stoichiometry of diffusing species. Mungall *et al.* (1998) considered that the coefficients themselves define the exchange process. This latter view has been adopted in this study to calculate the coefficients of the eigenvectors in Table 4. In our opinion, a change in concentration of oxide components in the proportions expressed by the eigenvectors does not necessarily mean that they form part of a melt species with that exact proportion, or even that they form part of a melt species. Alternative interpretations can be proposed. For example, where coupled diffusion is evident, covariations of elements might signify only that the migration of some chemical components induces structural changes in melt that require the movement of other components to accommodate them. This does not imply that these components are bonded or even nearest neighbors. Although diffusion studies are extremely important for pointing out structural features and possible species in melt, they are more meaningful when coupled with spectroscopic data on the melt or glass. For example, Wolf & London (1994) proposed that excess Al and P associate in haplogranitic melts in a ratio 1:1 as $AlPO_4$, based on diffusion experiments involving dissolution of apatite in the melt. Using various spectroscopic methods, Mysen *et al.* (1981*a*, 1999), Gan & Hess (1992) and Toplis & Schaller (1998) observed that Al is associated with P in granitic glasses as a nearest neighbor in the ratio 1:1 and so corroborated

the species $AlPO_4$. This example demonstrates that complex components identified as eigenvectors may represent actual melt species, and it is important that future studies assess the general validity of this conclusion with regard to other melt species.

If the chemical profiles and our analysis of them do correspond to a peraluminous melt species, then we deduce that this species is not simply alumina but is alumina coupled with alkalis and perhaps hydrogen for charge balance to yield an ASI of 1·20. The uniformity of the Al/Na ratio throughout melt columns of all experiments points to a strong chemical affinity between these two elements. Silica does not appear to be a component of the aluminum–alkali species, as the silica concentration profiles fit a simple pattern of dilution by the other moving components. If this concept can be validated (e.g. through spectroscopic or other methods), then haplogranitic melt could be viewed as consisting of at least two species, silica and alkali aluminate, where the stoichiometry of the alkali aluminate is simply the ASI and alkali ratio of the melt.

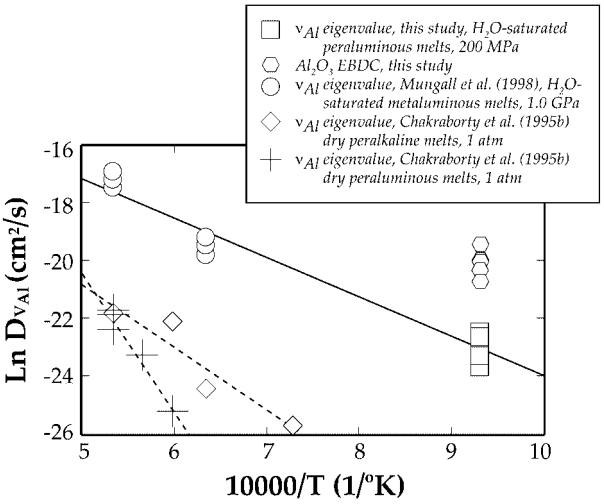

Fig. 16. Arrhenian plot for the EBDC of Al_2O_3 and the eigenvalues associated with v_{Al} calculated in this study. The v_{Al} eigenvalues calculated in previous studies involving similar or alike systems are also shown for comparison. Continuous line is the linear fit to the v_{Al} eigenvalues obtained in this study and by Mungall *et al.* (1998).

Comparison with previous experimental diffusion studies

Mungall *et al.* (1998) conducted diffusion couples experiments in the H_2O-saturated metaluminous haplogranite system at 1300–1600°C and 1·0 GPa along seven different directions in composition space. Although they found that the eigenvalues associated with the eigenvectors v_{Na}, v_K and v_H were degenerate to the degree of accuracy permitted by their analyses, they also found that the eigenvalues associated with v_{Na} and v_K are much larger than that associated with v_{Al}, and that diffusion of aluminum involves migration of alkalis and H_2O. These results are in agreement with our observations from the study of the concentration profiles. The stoichiometry of their v_{Al} (ASI of ~1·15 and Al/Na molar ratio of ~1·55) is slightly different from ours. We note, however, that their Al/Na ratio corresponds approximately to the mean Al/Na molar ratio in many of their diffusion couples (see their table 2). This is in accord with our suggestion that this molar ratio in v_{Al} will be controlled by the composition of the whole melt. Chakraborty *et al.* (1995*b*) calculated eigenvectors and eigenvalues in the system K_2O–Al_2O_3–SiO_2, at 1100–1600°C and atmospheric pressure, from diffusion couples experiments in both peraluminous and peralkaline compositions. They found potassium to be slightly coupled with aluminum.

Although these previous experimental studies were conducted at pressures very different from ours, we plotted the eigenvalues of v_{Al} obtained in the three studies versus the experimental temperature (Fig. 16). Despite the difference in pressures, the eigenvalues obtained in this study roughly follow the trend suggested by the data of Mungall *et al.* (1998). A linear fit to the data provides an activation energy of ~114·1 kJ/mol and a pre-exponential factor of $\sim 3{\cdot}48 \times 10^{-5}$ cm^2/s. The EBDC calculated for Al_2O_3 in this study, however, is clearly above the trend suggested by the data of Mungall *et al.* (1998). The v_{Al} eigenvalue calculated in this study at 800°C is similar to that obtained by Chakraborty *et al.* (1995*b*) in the H_2O-absent system K_2O–Al_2O_3–SiO_2 at much higher temperatures, ~1500°C.

GEOLOGICAL APPLICATIONS

Rates of equilibration between corundum or andalusite and melt

The mechanisms proposed here and the conclusions drawn from them provide a means of understanding the generation of peraluminous crustal melts at the grain-boundary scale. The primary purpose of this paper has been to gain a better understanding of how peraluminous minerals such as corundum and andalusite dissolve into granitic melt, and hence how diffusion of aluminum (and other components) controls the rate of equilibration and modifies the ASI of nominally metaluminous haplogranitic melt. Kinetic factors alone are not responsible for the low ASI values of anatectic melts derived from metapelitic assemblages (e.g. London *et al.*, 2001). Together, however, knowledge of the compositional dependence and the kinetics of dissolution for peraluminous minerals will permit fruitful composition- and time-specific modeling of melt generation in real rocks.

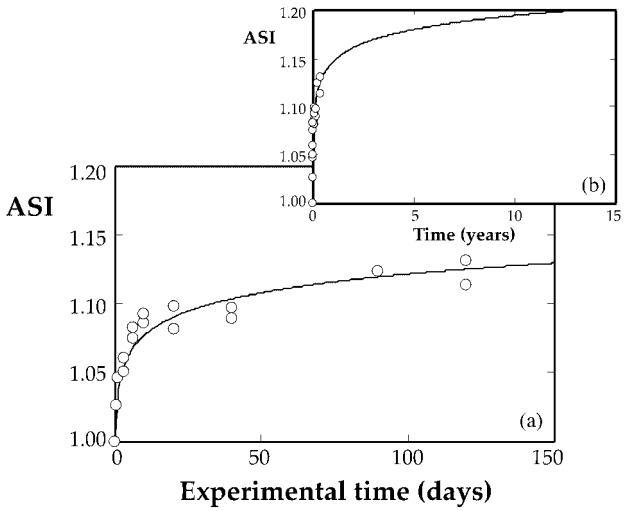

Fig. 17. (a) ASI vs time in the melt beyond the boundary layer of the corundum dissolution experiments. Each point represents the mean value of an analytical profile parallel to, and at 2000 or 3000–5000 μm from the interface. The data points are fitted to a power function. (b) Extrapolation of the power function to times where the ASI achieves a value of 1·20.

As first approximation to the time needed for H_2O-saturated haplogranitic melts to equilibrate with corundum or andalusite, we can use the calculated EBDC for Al_2O_3 or λ_{Al} and the following simple solution (Crank, 1975):

$$x^2 = Dt. \quad (9)$$

We will apply this model to a hypothetical rock in which two grains of corundum are connected by a narrow melt column 1 cm in length (and bordered, for example, by grains of quartz and feldspar, in which the melt is already saturated). The diffusion distance for the melt to reach equilibrium with the corundum grains is therefore 5 mm, equivalent to the longest melt columns used in these experiments. Using $D_{Al_2O_3(EB)} = 2{\cdot}0 \times 10^{-9}$ cm^2/s, equilibrium would be achieved in $\sim$5 years. λ_{Al} calculated by the multicomponent diffusion model, averaged as $1{\cdot}2 \times 10^{-10}$ cm^2/s, would predict attainment of equilibrium at $\sim$70 years. We compared these results with the evolution of the ASI beyond the boundary layer (at 2 and 4–5 mm from the corundum–melt or andalusite–melt interface) with time. The data fit a power function (Fig. 17) that, when extrapolated from the starting melt composition (ASI $\sim$ 1·00) to an ASI of 1·20, the ASI of H_2O-saturated haplogranitic melts at equilibrium with corundum or andalusite, predicts an equilibration time of $\sim$5–15 years. This is a long time on the scale of experimental studies, and hence slow diffusion—and the failure to achieve equilibrium between peraluminous minerals and melt—might explain some of the unexpectedly low ASI values reported from experiments (Fig. 1). These time frames, however, are short in a geological context, and they imply that the kinetics of alumina dissolution and diffusion will not play an important role in determining the final ASI values of anatectic melts if those melts are H_2O saturated. Diffusivity, however, may decrease up to three orders of magnitude at H_2O concentrations well below saturation in melt (e.g. Watson & Baker, 1991, and references therein). In that case, the same 5 mm melt column would achieve equilibrium in 10–100 kyr, which may be comparable with time frames in which the segregation of crustal melts may take place (Ayres *et al.*, 1997).

ACKNOWLEDGEMENTS

Support for this research was provided by National Science Foundation grants EAR-990165, INT-9603199, EAR-9618867, EAR-9625517 and EAR-9404658, and a postdoctoral grant to A.A.V. from the Universidad de Granada, Spain. We thank James Mungall and two anonymous referees for providing thorough reviews that improved the paper. We are grateful to Professor G. Bergantz for the editorial work and suggestions.

REFERENCES

Acosta, A. (1998). Estudio de los fenómenos de fusión cortical y generación de granitoides asociados a las peridotitas de Ronda. Ph.D. thesis, Universidad de Granada, Spain, 305 pp.

Acosta, A., Dewers, T. A. & London, D. (2000). Multi component diffusion and mineral dissolution in water saturated haplogranitic melts. *EOS Transactions, American Geophysical Union* **81**, 1295.

Acosta-Vigil, A., Pereira, M. D., Shaw, D. M. & London, D. (2001). Contrasting behavior of B during crustal anatexis. *Lithos* **56**, 15–31.

Ayres, M., Harris, N. & Vance, D. (1997). Possible constraints on anatectic melt residence times from accessory mineral dissolution rates: an example from Himalayan leucogranites. *Mineralogical Magazine* **61**, 29–36.

Baker, D. R. (1990). Chemical interdiffusion of dacite and rhyolite: anhydrous measurements at 1 atm and 10 kbar, application of Transition State Theory, and diffusion in zoned magma chambers. *Contributions to Mineralogy and Petrology* **104**, 407–423.

Barbero, L., Villaseca, C., Rogers, G. & Brown, P. E. (1995). Geochemical and isotopic disequilibrium in crustal melting: an insight from the anatectic granitoids from Toledo, Spain. *Journal of Geophysical Research* **100**, 15745–15765.

Barbey, P., Macaudiere, J. & Nzenti, J. P. (1990). High-pressure dehydration melting of metapelites: evidence from the migmatites of Yaoundé (Cameroon). *Journal of Petrology* **31**, 401–427.

Bea, F., Pereira, M. D. & Stroh, A. (1994). Mineral/leucosome trace-element partitioning in a peraluminous migmatite (a laser ablation-ICP-MS study). *Chemical Geology* **117**, 291–312.

Behrens, H. & Jantos, N. (2001). The effect of anhydrous composition on water solubility in granitic melts. *American Mineralogist* **86**, 14–20.

Bowen, N. L. (1921). Diffusion in silicate melts. *Journal of Geology* **29**, 295–317.

Bowen, N. L. (1928). *The Evolution of Igneous Rocks*. Princeton, NJ: Princeton University Press.

Braun, I., Raith, M. & Ravindra Kumar, G. R. (1996). Dehydration-melting phenomena in leptynitic gneisses and the generation of leucogranites: a case study from the Kerala Khondalite Belt, southern India. *Journal of Petrology* **37**, 1285–1305.

Chakraborty, S. (1995). Diffusion in silicate melts. In: Stebbins, J. F., McMillan, P. F. & Dingwell, D. B. (eds) *Structure, Dynamics and Properties of Silicate Melts. Mineralogical Society of America, Reviews in Mineralogy* **32**, 411–504.

Chakraborty, S. & Ganguly, J. (1992). Cation diffusion in aluminosilicates garnets: experimental determination in spessartine–almandine diffusion couples, evaluation of effective binary diffusion coefficients, and applications. *Contributions to Mineralogy and Petrology* **111**, 74–86.

Chakraborty, S., Dingwell, D. B. & Rubie, D. C. (1995*a*). Multicomponent diffusion in ternary silicate melts in the system K_2O–Al_2O_3–SiO_2: I. Experimental measurements. *Geochimica et Cosmochimica Acta* **59**, 255–264.

Chakraborty, S., Dingwell, D. B. & Rubie, D. C. (1995*b*). Multicomponent diffusion in ternary silicate melts in the system K_2O–Al_2O_3–SiO_2: II. Mechanisms, systematics, and geological applications. *Geochimica et Cosmochimica Acta* **59**, 265–277.

Chekhmir, A. S. & Epel'baum, M. B. (1991). Diffusion in magmatic melts: new study. In: Perchuk, L. L. & Kushiro, I. (eds) *Physical Chemistry of Magmas*. New York: Springer, pp. 99–119.

Clarke, D. B., McKenzie, C. B., Muecke, G. K. & Richardson, S. W. (1976). Magmatic andalusite from the South Mountain Batholith, Nova Scotia. *Contributions to Mineralogy and Petrology* **56**, 279–287.

Clemens, J. D. & Wall, V. J. (1981). Origin and crystallization of some peraluminous (S-type) granitic magmas. *Canadian Mineralogist* **19**, 111–131.

Cooper, A. R., Jr (1968). The use and limitations of the concept of an effective binary diffusion coefficient for multicomponent diffusion. In: Wachtman, J. B., Jr & Franklin, A. D. (eds) *Mass Transport in Oxides. National Bureau of Standards, Special Publication* **196**, 79–84.

Cooper, A. R., Jr & Kingery, W. D. (1964). Dissolution in ceramic systems: I, molecular diffusion, natural convection, and forced convection studies of sapphire dissolution in calcium aluminum silicate. *Journal of the American Ceramic Society* **47**, 37–43.

Cooper, A. R., Jr & Schut, R. J. (1980). Analysis of transient dissolution in CaO–Al_2O_3–SiO_2. *Metallurgical Transactions* **11**, 373–376.

Crank, J. (1975). *The Mathematics of Diffusion*. Oxford: Clarendon Press.

Davis, J. C. (1986). *Statistics and Data Analysis in Geology*. New York: Wiley.

Dingwell, D. B., Harris, D. M. & Scarfe, C. M. (1984). The solubility of H_2O in melts in the system SiO_2–Al_2O_3–Na_2O–K_2O at 1 to 2 kbars. *Journal of Geology* **92**, 387–395.

Dingwell, D. B., Holtz, F. & Behrens, H. (1997). The solubility of H_2O in peralkaline and peraluminous granitic melts. *American Mineralogist* **82**, 434–437.

Gan, H. & Hess, P. C. (1992). Phosphate speciation in potassium aluminosilicate glasses. *American Mineralogist* **77**, 495–506.

Gardien, V., Thompson, A. B., Grujic, D. & Ulmer, P. (1995). Experimental melting of biotite + plagioclase + quartz ± muscovite assemblages and implications for crustal melting. *Journal of Geophysical Research* **100**, 15581–15591.

Holdaway, M. J. & Mukhopadhyay, B. (1993). A reevaluation of the stability relations of andalusite; thermochemical data and phase diagram for the aluminumsilicates. *American Mineralogist* **78**, 298–315.

Holtz, F., Johannes, W. & Pichavant, M. (1992*a*). Peraluminous granites: the effect of alumina on melt composition and coexisting minerals. *Transactions of the Royal Society of Edinburgh: Earth Sciences* **83**, 409–416.

Holtz, F., Johannes, W. & Pichavant, M. (1992*b*). Effect of excess aluminum on phase relations in the system Qz–Ab–Or. Experimental investigation at 2 kbar and reduced H_2O activity. *European Journal of Mineralogy* **4**, 137–152.

Holtz, F., Behrens, H., Dingwell, D. B. & Johannes, W. (1995). H_2O solubility in haplogranitic melts: compositional, pressure, and temperature dependence. *American Mineralogist* **80**, 94–108.

Icenhower, J. & London, D. (1995). An experimental study of element partitioning among biotite, muscovite, and coexisting peraluminous silicic melt at 200 MPa (H_2O). *American Mineralogist* **80**, 1229–1251.

Icenhower, J. & London, D. (1996). Experimental partitioning of Rb, Cs, Sr, and Ba between alkali feldspar and peraluminous melt. *American Mineralogist* **81**, 719–734.

Joyce, D. B. & Voigt, D. E. (1994). A phase equilibrium study in the system $KAlSi_3O_8$–$NaAlSi_3O_8$–SiO_2–Al_2SiO_5–H_2O and petrogenetic implications. *American Mineralogist* **79**, 504–512.

Kontak, D. J., Clark, A. H. & Farrar, E. (1984). The magmatic evolution of the Cordillera Oriental, southeastern Peru. In: Harmon, R. S. & Barreiro, B. A. (eds) *Andean Magmatism. Chemical and Isotopic Constraints*. Nantwich: Shiva, pp. 203–219.

Lacy, E. D. (1963). Aluminum in glasses and in melts. *Physics and Chemistry of Glasses* **4**, 234–238.

Lange, R. A. & Carmichael, I. S. E. (1990). Thermodynamic properties of silicate liquids with emphasis on density, thermal expansion and compressibility. In: Nicholls, J. & Russell, J. K. (eds) *Modern Methods of Igneous Petrology: Understanding Magmatic Processes. Mineralogical Society of America, Reviews in Mineralogy* **24**, 25–64.

Le Breton, N. & Thompson, A. B. (1988). Fluid-absent (dehydration) melting of biotite in metapelites in the early stages of crustal anatexis. *Contributions to Mineralogy and Petrology* **99**, 226–237.

Lesher, C. E. (1994). Kinetics of Sr and Nd exchange in silicate liquids: theory, experiments, and applications to uphill diffusion, isotopic equilibration, and irreversible mixing of magmas. *Journal of Geophysical Research* **99**, 9585–9604.

Liang, Y. (1999). Diffusive dissolution in ternary systems: analysis with applications to quartz and quartzite dissolution in molten silicates. *Geochimica et Cosmochimica Acta* **63**, 3983–3995.

Liang, Y., Richter, F. M., Davis, A. M. & Watson, E. B. (1996). Diffusion in silicate melts: II. Multicomponent diffusion in CaO–Al_2O_3–SiO_2 at 1500°C and 1 GPa. *Geochimica et Cosmochimica Acta* **60**, 5021–5035.

Liang, Y., Richter, F. M. & Chamberlin, L. (1997). Diffusion in silicate melts: III. Empirical models for multicomponent diffusion. *Geochimica et Cosmochimica Acta* **61**, 5295–5312.

Linnen, R. L., Pichavant, M. & Holtz, F. (1996). The combined effects of f_{O_2} and melt composition on SnO_2 solubility and tin diffusivity in haplogranitic melts. *Geochimica et Cosmochimica Acta* **60**, 4965–4976.

London, D. (2001). The chemical signature of S-type granitic melts. In: Chappell, B. & Fleming, P. (eds) *S-type Granites and Related Rocks. Australian Geological Survey Organization Record* **2001/02**, 73–74.

London, D., Acosta, A., Dewers, T. A. & Morgan, G. B., VI (2001). Anatexis of metapelites: the ASI of S-type granites. *11th Annual Goldschmidt Conference Abstracts. Lunar and Planetary Institute Contribution* **1088**, Abstract 3363 (CD-ROM).

Montel, J. M. & Vielzeuf, D. (1997). Partial melting of metagreywackes, Part II. Compositions of minerals and melts. *Contributions to Mineralogy and Petrology* **128**, 176–196.

Morgan, G. B., VI & London, D. (1996). Optimizing the electron microprobe analysis of hydrous alkali aluminosilicate glasses. *American Mineralogist* **81**, 1176–1185.

Morgan, G. B., VI, London, D. & Luedke, R. G. (1998). Petrochemistry of late Miocene peraluminous silicic volcanic rocks from the Morococala field, Bolivia. *Journal of Petrology* **39**, 601–632.

Mungall, J. E., Romano, C. & Dingwell, D. B. (1998). Multicomponent diffusion in the molten system K_2O–Na_2O–Al_2O_3–SiO_2–H_2O. *American Mineralogist* **83**, 685–699.

Mysen, B. O., Ryerson, F. J. & Virgo, D. (1981*a*). The structural role of phosphorus in silicate melts. *American Mineralogist* **66**, 106–117.

Mysen, B. O., Virgo, D. & Kushiro, I. (1981*b*). The structural role of aluminum in silicate melts—a Raman spectroscopic study at 1 atmosphere. *American Mineralogist* **66**, 678–701.

Mysen, B. O., Holtz, F., Pichavant, M., Beny, J. M. & Montel, J. M. (1999). The effect of temperature and bulk composition on the solution mechanism of phosphorus in peraluminous haplogranitic magmas. *American Mineralogist* **84**, 1336–1345.

Noble, D. C., Vogel, T. A., Peterson, P. S., Landis, G. P., Grant, N. K., Jezek, P. A. & McKee, E. H. (1984). Rare-element-enriched, S-type ash-flow tuffs containing phenocrysts of muscovite, andalusite, and sillimanite, southeastern Peru. *Geology* **12**, 35–39.

Obata, M., Yoshimura, Y., Nagakawa, K., Odawara, S. & Osanai, Y. (1994). Crustal anatexis and melt migrations in the Higo metamorphic terrane, west–central Kyushu, Kumamoto, Japan. *Lithos* **32**, 135–147.

Oishi, Y., Cooper A. R., Jr & Kingery, W. D. (1965). Dissolution in ceramic systems: III, boundary layer concentration gradients. *Journal of the American Ceramic Society* **48**, 88–95.

Patiño Douce, A. E. (1992). Calculated relationships between activity of alumina and phase assemblages of silica-saturated igneous rocks. Petrogenetic implications of magmatic cordierite, garnet and aluminosilicate. *Journal of Volcanology and Geothermal Research* **52**, 43–63.

Patiño Douce, A. E. & Beard, J. S. (1996). Effects of P, $f(O_2)$ and Mg/Fe ratio on dehydration melting of model metagreywackes. *Journal of Petrology* **37**, 999–1024.

Patiño Douce, A. E. & Harris, N. (1998). Experimental constraints on Himalayan anatexis. *Journal of Petrology* **39**, 689–710.

Patiño Douce, A. E. & Johnston, A. D. (1991). Phase equilibria and melt productivity in the pelitic system: implications for the origin of peraluminous granitoids and aluminous granulites. *Contributions to Mineralogy and Petrology* **107**, 202–218.

Poe, B. T., McMillan, P. F., Coté, B., Massiot, D. & Coutures, J. P. (1992). SiO_2–Al_2O_3 liquids: *in situ* study by high temperature ^{27}Al NMR spectroscopy and molecular dynamics simulations. *Journal of Physics and Chemistry* **96**, 8220–8224.

Pouchou, J. L. & Pichoir, F. (1985). 'PAP' φ(ρz) correction procedure for improved quantitative microanalysis. In: Armstrong, J. T. (ed.) *Microbeam Analysis*. San Francisco, CA: San Francisco Press, pp. 104–106.

Richet, P., Whittington, A., Holtz, F., Behrens, H., Ohlhorst, S. & Wilke, M. (2000). Water and the density of silicate glasses. *Contributions to Mineralogy and Petrology* **138**, 337–347.

Robie, R. A., Hemingway, B. S. & Fisher, J. R. (1978). Thermodynamic properties of minerals and related substances at 298·15 K and 1 Bar (10^5 Pascals) pressure and at higher temperatures. *US Geological Survey Bulletin* **1452**, 456 pp.

Samaddar, B. N., Kingery, W. D. & Cooper, A. R., Jr (1964). Dissolution in ceramic systems: II, dissolution of alumina, mullite, anorthite, and silica in a calcium–aluminum–silicate slag. *Journal of the American Ceramic Society* **47**, 249–254.

Sato, H. (1975). Diffusion coronas around quartz xenocrysts in andesite and basalt from Tertiary volcanic region in northeastern Shikoku, Japan. *Contributions to Mineralogy and Petrology* **50**, 49–64.

Sato, R. K., McMillan, P. F., Dennison, P. & Dupree, R. (1991). A structural investigation of high alumina content glasses in the CaO–Al_2O_3–SiO_2 system via Raman and MAS NMR. *Physics and Chemistry of Glasses* **32**, 149–154.

Schairer, J. F. & Bowen, N. L. (1955). The system K_2O–Al_2O_3–SiO_2. *American Journal of Science* **253**, 681–746.

Schairer, J. F. & Bowen, N. L. (1956). The system Na_2O–Al_2O_3–SiO_2. *American Journal of Science* **254**, 129–195.

Shaw, C. S. (1999). Dissolution of orthopyroxene in basanitic magma between 0·4 and 2 GPa: further implications for the origin of Si-rich alkaline glass inclusions in mantle xenoliths. *Contributions to Mineralogy and Petrology* **135**, 114–132.

Shaw, C. S. (2000). The effect of experimental geometry on the mechanism and rate of dissolution of quartz in basanite at 0·5 GPa and 1350°C. *Contributions to Mineralogy and Petrology* **139**, 509–525.

Shaw, C. S. J., Thibault, Y., Edgar, A. D. & Lloyd, F. E. (1998). Mechanisms of orthopyroxene dissolution in silica-undersaturated melts at 1 atmosphere and implications for the origin of silica-rich glass in mantle xenoliths. *Contributions to Mineralogy and Petrology* **132**, 354–370.

Silver, L., Ihinger, P. D. & Stolper, E. (1990). The influence of bulk composition on the speciation of water in silicate glasses. *Contributions to Mineralogy and Petrology* **104**, 142–162.

Smith, V. G., Tiller, W. A. & Rutter, J. W. (1955). A mathematical analysis of solute redistribution during solidification. *Canadian Journal of Physics* **33**, 723–745.

Toplis, M. J. & Schaller, T. (1998). A ^{31}P MAS NMR study of glasses in the system xNa_2O–$(1 - x)Al_2O_3$–$2SiO_2$–yP_2O_5. *Journal of Non-Crystalline Solids* **224**, 57–68.

Torres-Roldán, R. L. (1983). Fractionated melting of metapelite and further crystal–melt equilibria. The example of the Blanca Unit migmatite complex, north of Estepona (southern Spain). *Tectonophysics* **96**, 95–123.

Trial, A. F. & Spera, F. J. (1994). Measuring the multicomponent diffusion matrix: experimental design and data analysis for silicate melts. *Geochimica et Cosmochimica Acta* **58**, 3769–3783.

Tubía, J. M. (1988). Estructura de los Alpujárrides occidentales: cinemática y condiciones de emplazamiento de las peridotitas de Ronda. *Publicaciones Especiales del Boletín Geológico y Minero de España* **99**, 124 pp.

Tuttle, O. F. & Bowen, N. L. (1958). Origin of granite in the light of experimental studies in the system $NaAlSi_3O_8$–$KAlSi_3O_8$–SiO_2–H_2O. *Geological Society of America Memoir* **74**.

Vielzeuf, D. & Holloway, J. R. (1988). Experimental determination of the fluid-absent melting relations in the pelitic system. *Contributions to Mineralogy and Petrology* **98**, 257–276.

Watson, E. B. (1982). Basalt contamination by continental crust: some experiments and models. *Contributions to Mineralogy and Petrology* **80**, 73–87.

Watson, E. B. & Baker, D. R. (1991). Chemical diffusion in magmas: an overview of experimental results and geochemical applications. In: Perchuk, L. L. & Kushiro, I. (eds) *Physical Chemistry of Magmas*. New York: Springer, pp. 120–151.

Watt, G. R. & Harley, S. L. (1993). Accessory phase controls on the geochemistry of crustal melts and restites produced during water-undersaturated partial melting. *Contributions to Mineralogy and Petrology* **114**, 550–566.

Weber, C., Barbey, P., Cuney, M. & Martin, H. (1985). Trace element behavior during migmatization. Evidence for a complex melt–residuum–fluid interaction in the St. Malo migmatitic dome (France). *Contributions to Mineralogy and Petrology* **90**, 52–62.

Wickham, S. M. (1987). Crustal anatexis and granite petrogenesis during low-pressure regional metamorphism: the Trois Seigneurs massif, Pyrenees, France. *Journal of Petrology* **28**, 127–169.

Wolf, M. B. & London, D. (1994). Apatite dissolution into peraluminous haplogranitic melts: an experimental study of solubilities and mechanisms. *Geochimica et Cosmochimica Acta* **58**, 4127–4145.

Zhang, Y. (1993). A modified effective binary diffusion model. *Journal of Geophysical Research* **98**, 11901–11920.

Zhang, Y., Walker, D. & Lesher, C. E. (1989). Diffusive crystal dissolution. *Contributions to Mineralogy and Petrology* **102**, 492–513.